m6A reader Pho92 is recruited co-transcriptionally and couples translation efficacy to mRNA decay to promote meiotic fitness in yeast

Radhika A. Varier[1,7,8], Theodora Sideri[1,7], Charlotte Capitanchik[1,7], Zornitsa Manova[1], Enrica Calvani[1], Alice Rossi[1], Raghu R. Edupuganti[2], Imke Ensinck[1], Vincent W.C. Chan[1], Harshil Patel[1], Joanna Kirkpatrick[1], Peter Faull[1,5], Ambrosius P. Snijders[1], Michiel Vermeulen[2], Markus Ralser[1,6], Jernej Ule[1,3], Nicholas M. Luscombe[1,4], and Folkert J. van Werven[1,8]

[1]The Francis Crick Institute, 1 Midland Road, London, NW1 1AT, UK

[2]Department of Molecular Biology, Faculty of Science, Radboud Institute for Molecular Life Sciences (RIMLS), Oncode Institute, Radboud University Nijmegen, 6525 GA Nijmegen, the Netherlands.

[3]Department of Neuromuscular Diseases, UCL Queen Square Institute of Neurology, Queen Square, London WC1N 3BG, UK; National Institute of Chemistry, Hajdrihova 19, 1001 Ljubljana, Slovenia.

[4]Department of Genetics, Evolution and Environment, UCL Genetics Institute, Gower Street, London WC1E 6BT, UK; Okinawa Institute of Science & Technology Graduate University, 1919-1 Tancha, Onna-son, Kunigami-gun, Okinawa 904-0495, Japan

[5]Biological Mass Spectrometry Facility, 2500 Speedway, The University of Texas at Austin, TX 78712

[6]Charité Universitätsmedizin Berlin, Department of Biochemistry, Germany

[7]These authors contributed equally

[8]Corresponding authors: radhikaav@gmail.com and folkert.vanwerven@crick.ac.uk

Abstract:

N6-methyladenosine (m6A) RNA modification impacts mRNA fate primarily via reader proteins, which dictate processes in development, stress, and disease. Yet little is known about m6A function in *Saccharomyces cerevisiae*, which occurs solely during early meiosis. Here we perform a multifaceted analysis of the m6A reader protein Pho92/Mrb1. Cross-linking immunoprecipitation analysis reveals that Pho92 associates with the 3'end of meiotic mRNAs in both an m6A-dependent and independent manner. Within cells, Pho92 transitions from the nucleus to the cytoplasm, and associates with translating ribosomes. In the nucleus Pho92 associates with target loci through its interaction with transcriptional elongator Paf1C. Functionally, we show that Pho92 promotes and links protein synthesis to mRNA decay. As such, the Pho92-mediated m6A-mRNA decay is contingent on active translation and the CCR4-NOT complex. We propose that the m6A reader Pho92 is loaded co-transcriptionally to facilitate correct translation and subsequent decay of m6A modified transcripts, and thereby promotes meiosis.

Introduction

Differentiation from one cell type to another requires accurate and timely control of gene expression. Molecular mechanisms of transcription, RNA processing and translation ensure precise temporal expression of genes. Over the last decade it has become evident that the fate of cells is also largely determined through RNA modifications (Roundtree et al., 2017). Specifically, the *N6*-methyladenosine (m6A) modification on messenger RNAs (mRNAs) has been shown to play a pivotal role in cell differentiation, development, and disease pathology (Yang et al., 2020).

The machinery that deposits m6A, also known as the m6A writer complex, consists of the catalytic subunit METTL3 and the catalytically inactive METTL14. Together they form the RNA binding groove, and are bound by WTAP and several other interacting proteins required to lay down the m6A mark on mRNAs (Liu et al., 2014). The m6A writer complex has strong preference for certain motifs (e.g. RRACH in mammals, and RGAC in yeast), and deposits m6A predominantly at the 3'end of transcripts (Dominissini et al., 2012; Meyer et al., 2012; Schwartz et al., 2013). Furthermore, the m6A mark is recognized and bound by reader proteins, which in turn recruit other protein complexes to control the fate of m6A marked transcripts (Zaccara et al., 2019). The YT521-B Homology (YTH) domain facilitates the m6A interaction of most m6A reader proteins, which defines the YTH family of proteins that is conserved from yeast to humans including plants (Patil et al., 2018). YTH domain containing proteins execute various mRNA fate functions, which includes mRNA decay, translation, transcription, and chromatin regulation (Lasman et al., 2020; Wang et al., 2014; Xiao et al., 2016; Zhou et al., 2015). Interestingly, YTH family proteins have been implicated both in translation and decay, suggesting that

these proteins may exert overlapping roles in regulating gene expression (Lasman et al., 2020; Wang et al., 2014; Wang et al., 2015; Zaccara and Jaffrey, 2020).

In yeast, the m6A modification occurs during early meiosis, as part of a critical developmental program known as sporulation (Clancy et al., 2002; Shah and Clancy, 1992). During sporulation, diploid cells undergo a single round of DNA replication followed by two consecutive nuclear meiotic divisions to produce four haploid spores (Figure 1A). Specifically, the m6A modification occurs during early meiosis (meiotic entry, DNA replication, prophase), and declines once cells undergo meiotic divisions (Schwartz et al., 2013) (Figure 1A). The deposition of m6A on mRNAs is catalysed by the methyltransferase Ime4, the Mettl3 orthologue. Ime4 also requires Mum2, the WTAP orthologue, and Slz1, which together comprise the m6A writer machinery in yeast called the MIS complex (Agarwala et al., 2012) (Figure 1A). Depending on the strain background, cells lacking Ime4 are either completely or severely impaired in undergoing meiosis and sporulation (Clancy et al., 2002; Hongay et al., 2006). Some evidence suggests that m6A contributes to the decay and translation of mRNAs (Bodi et al., 2015; Bushkin et al., 2019). However, the molecular function of the m6A modification in yeast remains largely unknown.

Here we dissected the function of m6A-dependent RNA binding proteins. By employing proteomics and individual-nucleotide resolution UV cross-linking and immunoprecipitation (iCLIP) analysis we reveal that Pho92/Mrb1 is likely the only m6A reader in yeast. Pho92 binds at 3’ ends of mRNAs in both an m6A dependent and independent manner. During early meiosis, Pho92 localizes to the nucleus, through its interaction with the RNA Polymerase II associated transcription

elongation complex, Paf1C, and transitions to the cytoplasm to associate with actively translating ribosomes. The Pho92 deletion mutant displays decreased decay of m6A modified mRNAs and increased aberrant nascent protein synthesis but not mature protein levels, indicating a role in translation and decay. We propose that Pho92 is part of an mRNA fate control pathway for m6A modified mRNAs that is instated during transcription and couples translation efficacy to mRNA decay, and thereby promotes gamete fitness in yeast.

Results

Pho92/Mrb1 is the sole m6A reader in yeast

To systematically identify proteins that interact with m6A in yeast, we incubated m6a modified RNA baits with cell extracts collected either pre-meiosis (PM) or during early meiosis (EM) (Figure 1A and 1B). We designed RNA baits consisting of four repeats of the canonical GGACU motif, that were either m6A modified (GGAmCU) or unmodified (GGACU) (Figure S1A) (Edupuganti et al., 2017). Subsequently, we performed differential labelling and mass-spectrometry (Figure S1A). We used the previously described synchronization method that relies on the induction of the master regulator Ime1 from the *CUP1* promoter (*pCUP-IME1*) to induce meiosis. We took the PM sample at 2 hours in sporulation medium (SPO) and EM sample at 4 hours in SPO, when the MIS complex is induced by Ime1 and consequently m6A occurs (Figure 1A and 1B) (Agarwala et al., 2012; Chia and van Werven, 2016; Schwartz et al., 2013).

We identified two proteins, Pho92 and Gis2, showing significant enrichment of binding to m6a modified baits compared to the unmodified bait. The most prominent

interactor Pho92, was specifically enriched during EM, whereas Gis2, was enriched in both PM and EM lysates (Figure 1C, Figure S1B, Table S4). Gis2 is an RNA binding protein that associates with ribosomes to facilitate translation by interacting with translation initiation factors (Rojas et al., 2012). Pho92, also known as methylation RNA binding protein 1 (Mrb1), has a conserved YTH domain that is required for its interaction with m6A (Schwartz et al., 2013; Xu et al., 2015). The molecular function of Pho92/Mrb1 in regulating the fate of m6A modified mRNAs is unknown.

To validate whether Gis2 and Pho92 bound preferentially to m6A *in vitro* we used recombinant proteins and performed RNA binding assays. Consistent with other reports (Schwartz et al., 2013; Xu et al., 2015), Pho92 associated with the m6A modified RNA oligo, but not with the unmodified control RNA oligo (Figure 1D). Gis2, however, displayed no binding to either modified or unmodified oligos in a repeating DRACH motif sequence context, though Gis2 binding was detected with a control RNA oligo harbouring its known binding motif of GA(A/U) repeats (Figure 1D and S1C). We assessed which region of Pho92 associates with the m6A modified RNA oligo by making truncations in the amino-terminal part (NΔ) of the protein, which is largely unstructured, and the YTH domain at the carboxy-terminus (YTHΔ). As expected, whilst removal of the amino-terminus had no impact on m6A modified oligo binding, removal of the YTH domain alone completely abrogated binding to the m6A modified oligo (Figure 1E).

Given that Pho92 was enriched only in early meiosis in the RNA pulldown, we assessed the expression of Pho92 protein and mRNA in asynchronous and

synchronized meiosis (Figure 1C, 1F and S1D). In line with proteomic analysis, we found that Pho92 was expressed only after the master regulator for entry into meiosis *IME1* was induced (Figure 1A, 1F and S1D). We examined whether the promoter of *PHO92* is possibly under direct control of Ume6, the DNA binding transcription factor that interacts with Ime1 to activate early meiosis gene transcription (Steber and Esposito, 1995). We found that the *PHO92* promoter harbours a canonical Ume6 binding site (CGGCGGCTA) 230 nucleotides (nt) upstream of the start codon, which displays strong binding of Ume6 (Chia et al., 2021)) (Figure 1G). Thus, Pho92 is expressed in early meiosis owing to its promoter being regulated by the meiosis-specific transcription factor Ime1 and its interacting partner Ume6.

Pho92 associates with mRNAs in an m6A dependent and independent manner

We next set out to determine the transcripts that Pho92 and Gis2 bind *in vivo*, their sequence and positional preferences, and to address whether this interaction is mediated by m6A. Specifically, we used a recently improved iCLIP protocol (Lee et al., 2021) to map Pho92 and Gis2 RNA binding sites during early meiosis (4h SPO). Gis2 crosslinked well to RNA with UV irradiation at 254 nm, whereas Pho92 elicited better crosslinking to RNA with UV irradiation at 365 nm in the presence of uracil analog, 4-thiouracil (4TU-iCLIP, Figure 1H and 1I) (Lee and Ule, 2018). Yeast cells lacking the sole m6A methyltransferase Ime4 display no detectable m6A signal during meiosis (Clancy et al., 2002; Schwartz et al., 2013). Therefore, we performed iCLIP in both wild-type and *ime4*Δ cells, to distinguish between Ime4-dependent and independent binding. To further assess whether the Ime4-dependent binding equates to specific binding of the reader protein to m6A sites, we performed m6A

individual-nucleotide-resolution cross-linking and immunoprecipitation (miCLIP) under the same growth conditions (Lee et al., 2021; Linder et al., 2015). By using our *ime4*Δ control we were able to distinguish bona fide m6A peaks from non-specific antibody binding. To control for changes in RNA abundance between wild-type and *ime4*Δ conditions, we also produced matched input libraries from mRNAs used for the miCLIP experiments, which also matched the timepoint used for the iCLIP experiments (4h SPO).

Due to the high proportion of cDNAs truncating at the peptide that is crosslinked to RNA fragments, we used the start positions of uniquely mapping reads to assign the positions of crosslink sites in iCLIP, and m6A sites in miCLIP (Lee and Ule, 2018). iCLIP and miCLIP replicate samples were highly reproducible at the level of counts per peak, clustering together in principle component analysis (PCA), with the greatest variance being due to the cells' genetic background (wild type (WT) or *ime4*Δ) (Figure S1E). However, it is notable that the proportion of variance accounted for by genetic background was much less for Gis2 (34%) than for the miCLIP (80%) or Pho92 (58%). For example, the *BDF2* transcript harboured several Pho92 binding sites that depended on Ime4, while Gis2 displayed m6A independent binding (Figure 1I).

We found 1286 miCLIP peaks in 870 genes that were reduced in *ime4*Δ cells (log2FoldChange <= -1, adjusted p value < 0.001), which we will hereby refer to as m6A sites (Figure 1J). Analysis of Gis2 iCLIP revealed 3563 peaks, of which only 43 peaks in 24 genes were decreased in *ime4*Δ representing only 1.2% of all Gis2 peaks (log2FoldChange <= -2, adjusted p value < 0.001) (Figure 1K). A much larger

number of Pho92 peaks (642 peaks in 507 genes, 16.7% of all detected peaks) were found to be reliably reduced in *ime4*Δ (log2FoldChange <= -2, adjusted p value < 0.001) (Figure 1L). Using a less stringent criteria we could designate up to 30% (1130/3823 peaks at log2FoldChange <= 0, adjusted p value < 0.05) of detected Pho92 peaks as reduced in *ime4*Δ, however for subsequent analysis we will refer to the 642 stringently defined peaks as "Ime4-dependent" Pho92 binding sites. This means that surprisingly, a large subset of Pho92 binding sites do not decrease in *ime4*Δ cells, indicating that Pho92 can also associate with transcripts in an Ime4 independent manner (Figure 1L). We ascertained that this is likely not background binding of Pho92 because in *ime4*Δ cells clear enrichment for Pho92-RNA complexes can be detected compared to the untagged control (Figure S1F). Indeed, when we implemented the iCLIP protocol to the untagged control, we found overall much less signal compared to the Pho92 iCLIP (Figure S1G).

To further explore whether Ime4-dependent Gis2 and Pho92 binding was also m6A-dependent, we calculated the distance to the nearest m6A site from each Ime4-dependent Gis2 and Pho92 binding site. To do so, we first validated our miCLIP data against published datasets (Garcia-Campos et al., 2019; Schwartz et al., 2013). As expected, m6A sites defined by miCLIP overlapped with m6A sites from the published datasets with ~30% of miCLIP m6A sites being within 50nt of a published site (Figure 1M and S1H). Similarly, Ime4-dependent Pho92 sites mapped close to m6A sites as determined by miCLIP or published data (Figure 1N and S1I). However, the few Ime4-dependent Gis2 binding events showed no clear proximity to m6A sites defined by either methodologies (Figure 1O and S1J). Further scrutiny of Pho92 binding revealed that the Ime4 dependent Pho92 association signal is highly

enriched at the m6A sites we identified using miCLIP (Figure S1K). We conclude that a substantial portion of Pho92 binding is dependent on m6A, while Gis2 binding to RNAs does not require the presence of m6A. Taken together, our data strongly suggest that Pho92 is likely the only m6A reader protein in yeast. For the remainder of this study we focus on our efforts to reveal the mechanism by which Pho92 controls the fate of m6A marked transcripts during yeast meiosis.

Features of transcripts bound by Pho92

Upon closer inspection of the Pho92 iCLIP data, we found that Pho92 iCLIP peaks are found in the mRNAs of key regulators of early meiosis such as *IME1* and *RIM4* (Figure 2A). The *IME1* and *RIM4* Pho92 iCLIP peaks overlapped with m6A sites identified with miCLIP (*RIM4*), or, in the case for *IME1*, with comparative Nanopore sequencing of WT versus *ime4*Δ described previously (Leger et al., 2021) (Figure S2A). Consistent with previous reports, *IME2,* a key kinase in meiosis, also displayed an Ime4-dependent peak in miCLIP data, though below our stringent thresholds (log2FC=-0.6, padj= 0.007) (Bodi et al., 2010; Schwartz et al., 2013) (Figure 2B). Interestingly, *IME2* displayed no detectable Pho92 binding, drawing our attention to the presence of m6A sites that are not bound by Pho92. In fact, while there was a good concordance between m6A sites and Pho92 binding, also prevalent were m6A sites where Pho92 was not detected and *vice versa* Pho92 binding sites with no detectable m6A site (Figure 2C). Differences between miCLIP, and iCLIP technique and protocols including data processing, can all contribute to such “missing overlaps”.

Using STREME, we analysed the RNA sequence context of Ime4-dependent Pho92 binding. Strikingly, the highest ranked motif found in Ime4-dependent Pho92 binding sites was nearly identical to the highest ranked motif found for the m6A sites, which highlights again that the Ime4-dependent sites are mostly m6A-dependent sites (Figure 2D, S2B and S2C). This motif is an “extended” RGAC sequence context, containing upstream AN and downstream NNU nucleotides that were previously described in (Schwartz et al., 2013).

As previously stated, consistent with the m6A pattern at mRNAs, Pho92 binding was detected predominantly at the 3’ end of transcripts, with 23% (145/642) of Ime4-dependent binding sites directly overlapping a STOP codon and 13% (410/3171) for Ime4-independent binding sites (Figure 2E and S2D). We also found Pho92 binding sites in the protein coding sequence or in 5’ end of transcripts, which included key meiotic mRNAs (*IME1* and *RIM4*) (Figure 2A and S2D). Although most transcripts contained just one m6A and/or a Pho92 binding site, some transcripts did contain two or more m6A and/or Pho92 binding sites (Figure 2F and 2G).

The Ime4-independent binding sites also showed positional enrichment at the 3’ end of mRNA transcripts, suggesting that these are likely bona fide binding sites (Figure 2E and S2D). Moreover, the Ime4-independent binding sites of Pho92 showed no enrichment for the m6A motif sequence but showed weak enrichment for short motif sequences containing GU dinucleotides, indicating that m6A independent binding of Pho92 is conceivably driven independent of sequence context (Figure 1H, S2B and S2C). Thus, Pho92 associates with transcripts predominantly at their 3’ ends, and a

subset of this binding occurs in an Ime4-dependent manner at m6A sites within canonical m6A motifs.

We performed gene ontology (GO) analysis of Pho92 bound transcripts (Ime4-dependent) and found that MAPK signalling, cell cycle and meiosis were the top enriched terms (Figure 2I). Notably, examination of m6A sites showed enrichment for MAPK signalling and cell cycle but not meiosis (Figure 2I), suggesting that m6A by itself regulates a different subset of transcripts than Pho92. Genes that showed Ime4-dependent Pho92 binding and corresponding m6A sites included those involved in regulating the meiotic program (such as *IME1*, *RIM4* and *SPO24),* DNA recombination and double strand-break repair (such as *HOP1* and *MEI5*) (Figure 2J and S2A).

Pho92 is important for the onset of meiosis and fitness of gametes

The yeast meiotic program is regulated by the master regulatory transcription factors, Ime1 and Ndt80 (van Werven and Amon, 2011). Ime1 drives early meiosis, while Ndt80 regulates the genes important for late meiosis, which includes meiotic divisions and spore formation (Chu et al., 1998; Kassir et al., 1988) (Figure 1A). GO-analysis of Pho92 bound transcripts revealed that Pho92 associates with genes important for meiosis. This posed the question whether Pho92 acts at the same genes as Ime1 and Ndt80, or perhaps regulates a different category of genes, independent of these two transcription factors. To identify Ime1 and Ndt80 regulated genes we performed RNA-seq in *ime1*Δ and *ndt80*Δ cells in early meiosis (4 hours in SPO). Subsequently, we compared the genes that were significantly downregulated in *ime1*Δ and *ndt80*Δ cells to Pho92 bound transcripts. We found that only 81 genes

out of the 507 Pho92 targets overlapped with the 1133 Ime1 regulated transcripts, while a meagre 54 genes overlapped with the 695 Ndt80 regulated transcripts (Figure 3A). Thus, a large fraction of transcripts bound by Pho92 were not direct targets of Ime1 or Ndt80. Similarly, little overlap was observed between m6A-marked transcripts and transcripts regulated by Ime1 or Ndt80 (Figure S3). Our data suggest that m6A and Pho92 regulate a distinct subset of transcripts or genes than the transcription factors (Ime1 and Ndt80) that control the meiotic program.

Given that Pho92 is specifically expressed during early meiosis (Figure 1D), we expect that, like Ime4, Pho92 plays a role in controlling gametogenesis. Therefore, we closely examined the effects of *pho92*Δ on meiosis and spore formation in the SK1 strain background, widely used for studying meiosis and sporulation. We found that *pho92*Δ exhibits a delay in the onset of meiosis compared to WT, though much milder than *ime4*Δ (Figure 3B). We found that the delay in meiotic divisions observed in *pho92*Δ cells was not alleviated by inducing *pCUP-IME1* (Figure 3C), supporting the idea that Pho92 and Ime1 regulate different subsets of genes. We also assessed whether Ndt80 expression can alleviate the effect of *pho92*Δ on meiosis. To do so, we expressed Ime1 and Ndt80 together when cells were starved in sporulation medium (SPO) (Figure 3D). We induced Ndt80 from the *GAL1-10* promoter (*pGAL-NTD80*) using the transcription factor Gal4 fused to estrogen receptor (Gal4ER) and addition of β-estradiol (Chia and van Werven, 2016). Expressing Ime1 and Ndt80 together surprisingly, had little effect on meiosis as most cells (more than 80%) completed at least one meiotic division after 8 hours after induction (Figure 3D). In *pho92*Δ cells about 50% of cells completed one meiotic division after 8 hours of

Ime1/Ndt80 induction (Figure 3D). Thus, the delay in meiosis in *pho92*Δ cells was not dependent on the expression of Ime1 and Ndt80.

We further assessed whether Pho92 contributes to the onset of meiosis in strain backgrounds that sporulate with a lower efficacy (S288C and A364A). Both S288C and A364A displayed more than 50 percent reduction in cells that underwent meiosis after 72 hours in SPO (Figure 3E and 3F). We further found that Pho92 contributes to the packaging of spores because the fraction of tetrads per asci decreased and the fraction of dyads increased in *pho92*Δ cells (Figure 3G). Finally, we quantified the effect of Pho92 on spore viability itself. We observed a modest reduction of spore viability when cells underwent sporulation at elevated temperatures (37°C) (Figure 3H). We conclude that the m6A reader Pho92 is important for the fitness of meiotic progeny in yeast.

Paf1C retains Pho92 in the nucleus during early meiosis

Proteins of the YTHDF family, to which Pho92 belongs, promote mRNA decay but have also been shown to impact translation efficiency, suggesting that there are overlapping roles (Li et al., 2017; Wang et al., 2014; Wang et al., 2015; Zaccara and Jaffrey, 2020). To identify a possible function for Pho92 in yeast, we determined its protein-protein interactions. We performed immunoprecipitation of Pho92 followed by label-free quantitative mass spectrometry. In addition to purifying Pho92 from cells staged in early meiosis, we also expressed Pho92 from heterologous promoters to intermediate levels (*CYC1* promoter, *pCYC1*-FLAG-Pho92) and to high levels (*PYK1* promoter, *pPYK1*-FLAG-Pho92) in cycling cells (Figure 4A, S4A-S4D). The purification of Pho92 from cells staged in early meiosis identified few interacting

proteins and weak enrichment for Pho92 itself (Figure S4A and S4C). In contrast, the purification from cycling cells grown in YPD identified large set of proteins that co-purified with Pho92 (Figure S4B and S4D). Specifically, several proteins involved in ribosomal biogenesis and translation were enriched compared to the untagged control (Figure 4A, S4D, and Table S6). Surprisingly, we also found that Pho92 interacted with proteins involved in chromatin organization and transcription. These included two subunits of RNA Polymerase II (pol II) associated transcription elongation complex Paf1C (Leo1 and Paf1), as well as the highly conserved and essential pol II associated transcription elongation factor Spt5 (Figure 4A).

To validate the interaction between Pho92 and Paf1C, we co-expressed epitope-tagged Pho92 and Paf1C and performed co-immunoprecipitation of Pho92 with Paf1C subunits Leo1 and Paf1 followed by western blotting. We found that Leo1, and to a lesser extent Paf1, co-immunoprecipitated with Pho92, but not the negative control hexokinase 1 protein (Figure 4B). Additionally, we affinity purified Pho92 fused to GST from *E. coli* and determined whether yeast extracts with HA-tagged Paf1, Leo1 or Ctr9 associated with recombinant GST-Pho92. We found that Paf1C subunits (Paf1, Leo1 and Ctr9) were enriched in the GST-Pho92 pull-down compared to the GST only or GST-Gis2 negative control, while the transcription factor Rap1 did not show enrichment (Figure 4C). We conclude that Pho92 interacts with Paf1C *in vitro* and *in vivo*.

Paf1C associates with pol II to promote transcription elongation and chromatin organization during transcription (Rondon et al., 2004; Van Oss et al., 2017). If Pho92 and Paf1C interact during meiosis, we hypothesized that Pho92 must localize

to the nucleus and possibly associate with gene bodies during transcription. To address this, we first determined whether the Paf1C regulates Pho92 localization in cells entering meiosis. To visualize Pho92 we tagged the protein with mNeongreen (Pho92-mNG) and monitored Pho92-mNG localization during a synchronized meiosis (*pCUP-IME1*). We determined nuclear Pho92 signal using histone H2B fused to mCherry (H2B-mCh) (Figure 4D). A large fraction of Pho92-mNG signal was in the nucleus prior to induction of meiosis (0h and 2h) and in the early time points of meiosis (3 and 4 hours) (Figure 4D and 4E (see WT)). At the later time points (5 and 6 hours), Pho92-mNG was however, largely excluded from the nucleus (Figure 4D and 4E (see WT)). It is noteworthy that the Pho92-mNG whole cell signal was lower prior to induction of meiosis (Figure S4E, S4F, and S4G). We conclude that Pho92 localization is dynamically regulated in cells undergoing early meiosis.

Next, we examined whether Paf1C contributed to Pho92 localization to the nucleus. We visualized Pho92-mNG localization in *leo1*Δ cells and in Paf1 depleted cells using the auxin induced degron (*PAF1-AID*) (Figure S4H). From 3 hours into sporulation onwards, we found that Pho92 was less nuclear in *leo1*Δ cells compared to the control (Figure 4E). A comparable difference in Pho92's nuclear localization was observed when we depleted Paf1 (*PAF1-AID* + IAA) (Figure 4F). We also examined whether Pho92 localization was dependent on the m6A writer Ime4. In *ime4*Δ cells Pho92 was retained more in the nucleus, indicating that m6A modified transcripts normally facilitate its exit from the nucleus (Figure 4G). We conclude that Pho92 localization is regulated throughout early meiosis. While Paf1C contributes to Pho92's localization to the nucleus, m6A modified transcripts facilitate transition of their reader Pho92 into the cytoplasm.

Paf1C directs Pho92 to target genes

Interaction between Leo1 and nascent mRNA has been reported to stabilize the association of Paf1C with transcribed genes (Dermody and Buratowski, 2010). Our data showing the effect of Paf1C on Pho92 localization to the nucleus raised the question of whether Pho92 is recruited to pre-mRNAs during transcription via Paf1C. To corroborate this idea that Pho92 associates with nascent mRNAs we scanned the iCLIP data for Pho92 association with intron regions which are typically retained in nascent mRNAs. We found 55 transcripts with Pho92 iCLIP signal in the intronic regions. For example, *BMH2* and *DMC1* intron regions contained Pho92 iCLIP crosslinks, while miCLIP and input displayed no detectable crosslinking within the intron sequence (Figure 4H and S4I).

To substantiate the observation that Pho92 associates with some of its targets during transcription, we performed Pho92 chromatin immunoprecipitation (ChIP) qPCR across two genes that contained Ime4-dependent Pho92 binding sites (*BDF2* and *GUT2*) (Figure 1G and 6A). In wild-type cells prior to entering meiosis (0 hours SPO), we found some Pho92 enrichment at these two ORFs (Figure 4I and 4J). Cells entering meiosis (3h SPO) showed an increase in Pho92 binding. Importantly, in *leo1*Δ cells Pho92 ChIP signal over the whole gene body was reduced (Figure 4I and 4J). This decrease cannot be attributed to Pho92 expression differences or meiotic defects because *leo1*Δ cells entered meiosis with a mild delay and expressed Pho92 to comparable levels as wild-type cells (Figure S4J and S4K). Also, the Paf1C deletion or depletion mutants we used for our experiments had little effect on cellular m6A levels (Figure S4L). Thus, Pho92 associates with target genes in a Paf1C-

dependent manner. Our data suggest that Pho92 is loaded co-transcriptionally to nascently produced mRNAs.

Pho92 interacts with ribosomes

The interaction between Pho92 and several ribosomal subunits observed in our IP-MS experiments (Figure 4A, Figure S4C, S4D, Table S6) prompted us to investigate whether Pho92 associates with ribosomes. We prepared cell lysates enriched for ribosomes from cells expressing *pPYK1*-FLAG-Pho92 by pelleting extracts with high-speed centrifugation. We observed that the majority of Pho92 sedimented together with ribosomes in the pellet (Figure 5A and Figure S5A). Additionally, we performed polysome profiling to determine whether Pho92 associates with actively translating ribosomes both in *pPYK1*-FLAG-Pho92 cycling cells and in diploid cells undergoing early meiosis (Figure S5B and S5C). In both conditions we found that Pho92 associates with polysome fractions as well as monosome fractions (Figure 5B and Figure S5C). We conclude that Pho92 can associate with active ribosomes. Notably, Pho92 association to ribosomes is likely at least partially independent of m6A as we found Pho92 associates with polysomes even in cycling cells, where there are little to no m6A modified transcripts present.

Pho92 stimulates translation efficacy

Our observation that Pho92 associates with ribosomes presented the possibility that Pho92 regulates translation. To investigate, we assessed the translation efficiency of Pho92-bound transcripts. We took a published data set and compared the translation efficiency of Pho92 targets throughout meiosis (Brar et al., 2012). We observed that the iCLIP targets of Pho92 such as *BDF2*, *RIM4* and *GUT2*, displayed increased

ribosome footprints specifically during pre-meiotic DNA replication and recombination (Figure 5C and S5D). Indeed, the median translation efficiency (TE) was higher for Pho92 target transcripts (Pho92 iCLIP) and m6A modified transcripts (miCLIP) during premeiotic DNA replication, and recombination compared to a control set of transcripts (Figure 5D). This increase in TE was more pronounced in transcripts possessing two or more Pho92 binding sites compared to just one (Figure 5E).

To determine whether Pho92 and m6A control translation, we examined polysome profiles and measured nascent protein synthesis. We noticed a small but reproducible effect on monosome over polysome ratio indicating a defect in translation in *pho92*Δ and *ime4*Δ cells (Figure 5F and Figure S5E). In addition, nascent protein synthesis was significantly increased in *pho92*Δ cells (Figure 5G and S5F). A possible explanation for this paradoxical result is that Pho92 prevents aberrant nascent peptide chain synthesis. This is in line with the idea that impaired mRNA quality control is directly linked to enhanced cotranslational ubiquitylation and protein misfolding (Duttler et al., 2013). *pho92*Δ cells displayed an increase in cotranslational ubiquitination compared to control cells suggesting Pho92 limits aberrant nascent protein synthesis (Figure 5H and S5G). These data indicate that Pho92 function is linked to translation and possibly to mRNA and protein quality control.

To further probe the role of Pho92 in protein synthesis, we performed differential gene expression analysis at the transcriptome level using RNA-seq and protein level using quantitative proteomics in WT and *pho92*Δ cells during early meiosis (Figure

5I, 5J and Figure S5H). We examined genes identified to have Ime4-dependent binding of Pho92 and also a control set of genes and assessed whether mature protein level changes were linked to changes in RNA expression. We reasoned that if Pho92 stimulates protein synthesis then in *pho92*Δ cells the protein over RNA ratio must be lower. To highlight differences, we grouped the RNA-seq data (WT vs *pho92*Δ) into three categories: genes that were down-regulated, showed little change or were up-regulated. For Pho92-bound transcripts, protein and RNA changes were not notably different for the group of genes that were down-regulated or showed little change in the RNA-seq (*pho92*Δ vs WT) (Figure 5I and Figure S5H). However, genes that were up-regulated in the RNA-seq (*pho92*Δ vs WT), were not upregulated for the protein products (Figure 5I). In contrast, the control set of genes that were up-regulated in the RNA-seq (*pho92*Δ vs WT), showed an increase in protein levels (Figure S5H). We noticed that the increase in the RNA-seq (*pho92*Δ vs WT) of this control group was less compared to Pho92-bound transcripts. This prompted us to generate a second control set of genes that showed approximately equal increase in the RNA-seq (*pho92*Δ vs WT) but no binding of Pho92. This control group of genes also showed an increase in protein levels following the RNA-seq (*pho92*Δ vs WT), while the Pho92-bound transcripts displayed a small decrease in protein level (Figure 5J). We conclude that Pho92-bound transcripts with increased RNA levels were not followed by an increase in protein levels in *pho92*Δ cells, supporting the idea that Pho92 stimulates accurate protein synthesis of its target mRNAs.

Pho92 and Paf1C contributes to translation efficacy of targets

To confirm if the aforementioned trend of discordant protein and mRNA levels can also be observed for individual genes, we selected several transcripts with Ime4-

dependent Pho92 binding sites to test further (Figure 6A and 1D). We tagged *INO1*, *SRT1, GUT2* and *BDF2* genes either at the amino-terminus seamlessly with sfGFP or at the carboxy-terminus with a V5 epitope tag. Subsequently, we performed time courses covering early meiosis from cells either directly shifted to starvation (SPO medium) or used *pCUP1-IME1* to induce meiosis in a highly synchronous manner. As a control, we included the *IME2* gene where we observed no detectable Pho92 binding despite the presence of m6A signal (Figure 2B).

For each time course experiment, we determined the relative protein levels, RNA levels, and as a proxy for translation efficacy we computed the protein over RNA ratio. Consistent with the proteomics and RNA-seq data, we found that *RGT1*, *INO1*, *SRT1*, *BDF2* and *GUT2* displayed a marginal but consistent decrease in protein over RNA levels in *pho92*Δ cells over several time points (Figure 6B-6G and S6A-S6F). For example, *SRT1* showed increased RNA levels in *pho92*Δ cells compare to the control, while protein levels were higher in control cells (Figure 6B and S6A). In contrast the negative control, *IME2*, showed no decrease in protein over RNA ratios in *pho92*Δ cells (Figure 6C and S6B). Like *SRT1*, the protein over RNA ratios decreased for *RGT1* and *GUT2* in *pho92*Δ cells (Figure 6D, 6E, S6C, and S6D). In experiments where *pCUP-IME1* was induced for synchronization we also observed that the protein over RNA ratios of *INO1* and *BDF2* were decreased in *pho92*Δ cells compared to the control at later time points (Figure 6F-6G, S6E, and S6F). The effect on *BDF2* was mild, but it is noteworthy that the V5-tag at the carboxy terminus (*BDF2*-V5) probably affects Pho92 binding at the 3' UTR.

Vice versa, we examined whether overexpression of Pho92 can have the opposite effect on translation efficacy. We expressed Pho92 to high levels from the *CUP1* promoter (*pCUP-PHO92*) and measured protein and RNA levels for *GUT2* (Figure S6G). We chose *GUT2* because the iCLIP analysis showed a clearly defined Pho92 peak in the 3' UTR, and both the protein and RNA levels were affected in *pho92*Δ cells. In the presence of high levels of Pho92 (*pCUP-PHO92* + Cu) we observed an increase in Gut2 protein levels while RNA levels decreased, and consequently a substantial increase in protein over RNA ratio (Figure 6H and S6G). The effect was dependent on the presence of Ime4 (Figure 6H and S6G). Overexpression of Pho92 had no effect on Ime2 protein over RNA ratios (Figure 6I and S6H).

To establish a link between the co-transcriptional loading of Pho92 to mRNAs and its eventual function of promoting protein production (Figure 4), we examined how Pho92 targets are affected in *leo1*Δ cells. Specifically, we examined RNA and protein levels of *GUT2* and *BDF2* throughout early meiosis. We found that the protein over RNA ratios were lower at 2 and 3 hours in SPO (Figure 6J-K and S6I-J). We hence conclude that Pho92 associates with ribosomes to stimulate protein synthesis and this is dependent on its co-transcriptional recruitment by Paf1C.

Pho92 limits the accumulation of m6A modified transcripts

Translation and mRNA decay are coupled to facilitate uptake of mRNA into the protein production cycle and then mRNA clearance. In mammalian cells YTH containing m6A reader proteins have been directly linked to the decay of m6A marked transcripts (Zaccara and Jaffrey, 2020). Additionally, mammalian m6A readers YTHDF3 and YTHDC2, like Pho92, associate with ribosomes and promote

translation (Li et al., 2017; Mao et al., 2019). Our data suggests that Pho92 plays a direct role in stimulating translation. However, some Pho92 targets (e.g. *SRT1* and *GUT2*) showed clear upregulation of mRNA levels in *pho92*Δ cells, indicating a perturbation of the mRNA decay pathway as well (Figure 6B and S6D).

This prompted us to examine whether Pho92 function is also linked to mRNA decay. First, we analysed RNA-seq data (*pho92*Δ vs WT) of cells staged prior to meiosis when Pho92 is not expressed (0 hours SPO) or undergoing early meiosis when Pho92 is induced (4 hours SPO). We specifically examined the Pho92 Ime4-dependent transcripts identified by iCLIP. At 0 hour in SPO, we observed little difference between *pho92*Δ and the WT (Figure 7A and S7A). At 4 hours in SPO we observed a small but notable increase in expression for Pho92 bound transcripts (Figure 7A and S7A). Out of 295 transcripts significantly up-regulated in *pho92*Δ vs WT (4 hours SPO), 95 were Pho92 targets as determined by iCLIP (Figure S7A). Likewise, transcripts significantly upregulated in *pho92*Δ at 4 hours in SPO showed greater binding of Pho92 at 3'ends compared to genes that either did not change in expression or were downregulated (Figure 7B). We observed similar correlations of Pho92 binding with changes in expression in the *ime4*Δ cells (Figure S7B-S7D).

We reasoned that if Pho92 is indeed important for the decay of m6A modified transcripts, *pho92*Δ cells should display higher m6A levels. Hence, we determined the m6A levels by LC-MS of cells entering meiosis (4h SPO) and compared the wild type to *pho92*Δ. We found that mRNAs isolated from *pho92*Δ cells displayed a marked increase in m6A over adenosine (A) levels (Figure 7C). As expected, *ime4*Δ cells showed no detectable m6A levels.

Given that Pho92 also localized to the nucleus and transitions to the cytoplasm and associated with ribosomes, it is plausible that Pho92 regulates the transport of transcripts. If Pho92 is primary involved in transport, then in *pho92*Δ cells Pho92 mRNA targets must be more depleted at translating ribosomes. However, if Pho92 primary regulates post-transcriptional mRNA clearance then we expect that Pho92 target transcripts that are not directed for decay will be upregulated at translating ribosomes in *pho92*Δ cells. To address this, we isolated ribosomes by polysome fractionation and performed RNA-seq on RNA isolated from polysomes fraction and compared this to RNA isolated from whole cell extracts. However, the Pho92 iCLIP targets were similarly upregulated in the polysome fraction and in whole cells (*pho92*Δ vs WT, 4 hours SPO) (Figure 7D). The polysome RNA-seq analysis indicates a plausible role for Pho92 in mRNA decay during or post translation and moreover suggests that Pho92 is likely not important for mRNA transport.

CCR4-NOT represses the levels of m6A marked transcripts

Pho92 itself has no known enzymatic activity that would drive the decay of transcripts. To identify protein complexes involved in the decay of m6A modified transcripts via Pho92, we depleted or deleted various genes involved in mRNA decay, and measured the effect on m6A levels via LC-MS in meiosis (6h SPO) (Figure 7E and 7F). Essential components were depleted using the induction of the AID system at 4 hours in SPO and m6A levels were determined at 6 hours SPO (2 hours after depletion). We also compared the LC-MS data with m6A-seq2 data, a technique that relies on multiplexed m6A-immunoprecipitation of barcoded and pooled samples, of the same depletion alleles (Dierks et al., 2021). Depletion of

Caf40 and Rat1 (*CAF40-AID* and *RAT1-AID*) showed a consistent increase in m6A levels using both LC-MS and m6A-seq2 (Figure 7E). In contrast depletion of Xrn1 (*XRN1-AID*) had the opposite effect and showed reduced m6A levels. We also found that *not3*Δ displayed an increase in m6A levels detected by LC-MS and m6A-seq2 (Figure 7F). Our data suggest that the various mRNA decay pathways can have opposing effects on m6A levels during yeast meiosis.

Pho92-CCR4-NOT promote m6A decay in a translation dependent manner

We found that Pho92 and Not3 deletion mutants as well as depletion of Caf40 resulted in increased levels of m6A modified transcripts possibly via the CCR4-NOT complex. Both Caf40 and Not3 are part of the CCR4-NOT complex the major mRNA deadenylation complex in eukaryotes (Collart, 2016). Various reports have shown that YTH reader proteins facilitate recruitment of the CCR4-NOT complex to target RNAs (Du et al., 2016; Kang et al., 2014). In yeast, a direct interaction between CCR4-NOT and Pho92 has been reported, but no link with m6A marked transcripts has been established (Kang et al., 2014).

Therefore, we decided to assess the relative decay rate of m6A modified transcripts and the contribution of Pho92 and CCR4-NOT complex directly. We reasoned that if m6A modified transcripts are less stable compared to non-m6A mRNAs, m6A is expected to decay faster after blocking mRNA synthesis. We treated cells with thiolutin to block transcription, and subsequently determined m6A levels by m6A-ELISA or LC-MS (Figure 7G and S7E). m6A levels indeed declined faster after blocking transcription with thiolutin. Consistent with the hypothesis that Pho92 promotes decay, in *pho92*Δ cells we observed little to no decline in m6A levels after

blocking transcription. Since Pho92 co-purifies with ribosomes (Figure 5), we next examined whether the decay of m6A modified transcripts relied on active translation. We blocked both transcription and translation by treating cells with thiolutin and cycloheximide. Blocking transcription and translation alleviated the differences in decay rates between *pho92*Δ and wild-type cells, suggesting that the decay of m6A modified transcripts is certainly dependent on translation (Figure 7H and S7E). We conclude that Pho92 promotes decay of m6A marked transcripts at translating ribosomes.

Next, we determined whether the CCR4-NOT complex had a similar effect on the decay of m6A modified transcripts as Pho92. We blocked transcription in *not3*Δ diploid cells entering meiosis, and measured m6A levels. We found that like Pho92, the decay of m6A-modifed transcripts was reduced in *not3*Δ diploid cells when compared to wild-type cells (Figure 7I and S7F). Similarly, blocking translation and transcription alleviated the differences between *not3*Δ and wild type (Figure S7F). Thus CCR4-NOT facilitates the decay of m6A modified transcripts. Given that CCR4-NOT and Pho92 interact with each other, our data suggest that Pho92 promotes decay of its target transcripts via the CCR4-NOT complex. We propose that Pho92 stimulates the translation coupled decay of transcripts to drive efficient protein production of m6A modified transcripts (Figure 7J).

Discussion

m6A modified transcripts are abundant during early yeast meiosis, yet the function of the m6A mark remains elusive. Here we show that the YTH domain containing protein Pho92/Mrb1 is likely the only m6A reader in yeast and is critical for the onset

of meiosis and fitness of gametes. Importantly, we provide evidence that Pho92 co-transcriptionally associates with mRNAs to direct m6A-modifed transcripts for their translation to decay fate. Our study further shows that Pho92 promotes efficient protein synthesis of m6A modified transcripts by coupling translation efficacy to mRNA decay (Figure 7J). Our work in yeast meiosis establishes a link between the previously described decay and translation functions of YTH reader proteins and m6a modified mRNAs.

Pho92 is key to meiotic fitness

During yeast meiosis, which is induced by severe nutrient starvation, diploid cells are triggered to undergo inarguably the most complex cell differentiation program of the yeast life cycle (Neiman, 2011; van Werven and Amon, 2011). Master transcription factor Ime1, which drives the transcription of genes in early meiosis, likely directly regulates *PHO92* transcription. Thus in yeast the m6A writer and reader machinery (Pho92 and the MIS complex) are specifically induced during early meiosis (Figure 7J). Interestingly, Pho92 also regulates the stability of the *PHO4* transcript in a phosphate-dependent manner, suggesting that Pho92 may also play an additional role outside meiosis when there is no m6A (Kang et al., 2014).

Tight regulation of gene expression is critically important to ensure no cellular resources are wasted during meiosis. With this view, the role of Pho92 in coupling translation efficacy to mRNA decay provides an elegant strategy to facilitate increased protein synthesis and subsequent decay of mRNAs important for meiosis. One other possibility is that Pho92 is important for decay of mitotic transcripts, so that cells can enter gametogenesis, or decay of early meiotic transcripts, so that cells

enter the subsequent stages of gametogenesis. If this is the case, one expects to find the m6A modified transcripts to be confined to a defined stage corresponding to either the exit from mitosis or entry into meiotic divisions. However, we observe no enrichment for genes linked to mitosis in the Pho92 iCLIP data, and m6A levels are spread over several stages during early meiosis (Schwartz et al., 2013). Rather, our data suggests that Pho92 increases the translation efficacy of m6A modified transcripts during critical stages of the early meiotic program when errors in meiotic chromosome segregation are fatal to the survival of gametes. Indeed, cells lacking Pho92 exhibit a delay in the onset of meiotic divisions and reduced gamete fitness.

While Pho92 deletion mutants exhibit a delay in meiosis, an Ime4 deletion mutant has more severe phenotype (Figure 3). Apart from the function that m6A has to mediate the Pho92 interaction, it is plausible that m6A has additional roles. However, it is worth noting that a catalytic dead mutant of Ime4 has a less severe phenotype in meiosis, which lead to the conclusion that Ime4 has noncatalytic function during meiosis (Agarwala et al., 2012). Therefore, we propose that the implications of the m6A modification is largely manifested through Pho92.

Mechanism of co-transcriptional loading of Pho92

Our data suggests that Pho92 interacts with target transcripts during transcription via transcription elongator Paf1C (Figure 7J). First, we found that Pho92 can interact with Paf1C, and that this interaction is critical for the localisation of Pho92 to the nucleus. Interestingly, the Leo1 subunit of Paf1C is also known to interact with nascent RNA, and thus forms a logical platform to facilitate the interaction between Pho92 and nascent RNA (Dermody and Buratowski, 2010). Pho92 binding sites

show striking 3' end enrichment regardless of whether binding is Ime4-independent or at m6A sites, which would suggest that the positioning is not entirely dependent on m6A. Pho92 accumulates at chromatin over the course of gene transcription, in a manner that is dependent on Paf1C. This would suggest that transcription or chromatin factors contribute towards Pho92 positioning on transcripts, which may explain why Ime4-independent Pho92 binding does not need a strong RNA sequence context. A simple mechanism could be that m6A locks Pho92 binding to RNA, which in turn allows the Pho92-mRNAs to be sent to translating ribosomes (Figure 7J). It is likely that without m6A locking Pho92 in place, the protein-RNA interaction is less stable.

Paf1C has also been reported to possess a more generic role in controlling the fate of transcripts in export (Fischl et al., 2017). Given that Pho92 resides in the nucleus during early meiosis, it is possible that Pho92 is important for export. However, RNA-seq of polysomes showed that Pho92 targets still associate with active ribosomes in the Pho92 deletion mutant (Figure 7D), which refutes a role in transport for Pho92. We propose that co-transcriptional association of Pho92 to mRNAs sets up the fate of mRNA early in the mRNA life cycle. As such, we show that *leo1*Δ affects the protein over RNA ratios for at least two target genes (Figure 6), despite the possibility of redundancy among the Paf1C subunits. However, further molecular analysis is needed to decipher this intriguing link between Paf1C, Pho92, and the fate of RNAs.

Transcription and chromatin mediated loading of RNA binding proteins and m6A machinery to control RNA fates is not only limited to Pho92. The co-transcriptional

loading of RNA binding proteins has been reported for other RNA binding proteins to control RNA export (Shahbabian et al., 2014; Viphakone et al., 2019). There is also evidence that the promoter sequences influence the stability of RNA (Trcek et al., 2011). With regard to m6A, there is proof that m6A is deposited early in RNA synthesis either co-transcriptionally or via chromatin (Huang et al., 2019; Ke et al., 2017). YTH proteins can act in the nucleus to facilitate the decay of nuclear m6A modified transcripts and thereby control chromatin states (Liu et al., 2020). In *S.pombe*, the YTH-RNA-binding protein Mmi1 is also reported to be co-transcriptionally recruited to 'decay-promoting' introns bearing sequence elements known as 'determinants of selective removal' (DSRs), which are enriched in meiotic mRNAs (Kilchert et al., 2015). Contrary to other known YTH-containing domain proteins including Pho92, Mmi1 is incapable of binding to the m6A consensus motif and the Mmi1 role is in fact reported to be suppression of activation of the meiotic programme during mitotic growth, which is in contrast to Pho92's role in meiosis in *S. cerevisiae* (Harigaya et al., 2006; Shichino et al., 2018; Wang et al., 2016).

The role of Pho92 in the translation to decay fate

Our analysis of Pho92 shows that the destiny of m6A marked transcripts in translation and mRNA decay are linked. On one hand, we have experimental evidence showing Pho92 is important for efficient protein production. Deletion of Pho92 leads to a reduction in protein over RNA ratios, suggesting translational efficacy is lowered. Additionally, Pho92 bound transcripts showed increased translation efficiency compared to a control set (Figure 5). On the other hand, Pho92 stimulates the decay of m6A modified transcripts. How does Pho92 promote decay as well as translation efficacy of m6A modified transcripts? While it is not impossible

that the translation and decay functions of Pho92 are exerted via distinct mechanisms, the likelihood of these functions being linked is more plausible. Firstly, the decay of m6A marked transcripts bound by Pho92 occurred in a translation dependent manner. Secondly, we found that Pho92 associates with actively translating ribosomes, limits aberrant nascent protein synthesis, and is directly linked to increased translation efficacy. Thirdly, our analysis of decay mutants revealed that the CCR4-NOT complex facilitates the decay of m6A marked transcripts (Figure 7J). Specifically, depleting the Not3 and Caf40 subunits resulted in increased m6A levels. CCR4-NOT is the major deadenylase complex in cells, which acts at ribosomes and facilitates co-translational decay (Collart, 2016). Though we did not establish a direct interaction between Pho92 and the CCR4-NOT complex in this study, others have shown that Pho92 interacts with the Pop2 subunit of CCR4-NOT (Kang et al., 2014).

In mammalian cells, YTHDF1 and YTHDF2 have been implicated in translation and decay, respectively (Wang et al., 2015; Zaccara and Jaffrey, 2020). Also YTHDC2 has been assigned both functions in decay and translation (Hsu et al., 2017; Kretschmer et al., 2018; Mao et al., 2019). Thus, opposite effects have been reported for YTH reader proteins. YTHDF2, the likely orthologue of Pho92, has been shown to be important for oocyte development, where it is important for decay of maternal RNAs (Ivanova et al., 2017). YTHDF2 associates with CCR4-NOT in mammalian cells (Du et al., 2016). Thus, the link between CCR4-NOT, YTH domain-containing proteins and m6A is likely conserved in yeast and mammalian gametogenesis. Interestingly, the translation function of YTHDF1 has been disputed, and it has been proposed that YTHDF proteins act redundantly to regulate decay (Zaccara and Jaffrey, 2020). Contradicting this, a significant enrichment of m6A in

yeast ribosomal fractions and increased methylation of the most efficiently translated transcripts in the early stages of meiosis has been reported (Bodi et al., 2015). Perhaps, the decay functions of Pho92 and YTHDF1 at ribosomes facilitates translational efficiency and as consequence decay or *vice versa*. The reason that mammalian studies have failed to conclude that decay and translation functions may go hand in hand is perhaps because mammalian studies of YTH proteins have typically focused on cell lines under steady state conditions (Zaccara and Jaffrey, 2020). In contrast, yeast meiosis is a dynamic process requiring extremely quick turn over of cell RNA and protein states, which is made possible by tightly coupled RNA decay and translation.

More and more studies show that an intimate link between translation and decay exists (Pelechano et al., 2015; Presnyak et al., 2015). Slowing down translation elongation has been linked to slowing the decay of transcripts (Chan et al., 2018). Perhaps, Pho92 directly promotes translation elongation, which in turn leads to faster decay via the CCR4-NOT complex. As such, there is evidence that CCR4-NOT complex, apart from its direct function in translation coupled decay, monitors translating ribosomes for codon optimality (Buschauer et al., 2020). Another intriguing possibility is that m6A and Pho92, together with CCR4-NOT are part of an mRNA quality control mechanism to limit aberrant protein synthesis and protein misfolding, while at the same time increase productive translation. In line with this idea is that YTHDC2 protein facilitates interactions between m6A, ribosomes, and decay factors to control stability and translation of the mRNAs, and together possibly constitutes an mRNA to protein quality control mechanism (Inada, 2020; Kretschmer et al., 2018). How m6A, Pho92 and CCR4-NOT together promote translation and

decay and how this is linked to a quality control for mRNAs and aberrant translation remains subject for further investigation.

YTH reader proteins are conserved from yeast to humans and play critical roles in developmental programs and disease pathogenesis (Patil et al., 2018). YTHDF1 has been shown to be involved in tumour cells immune evasion, while YTHDF2 promotes tumour cell proliferation (Chen et al., 2017; Han et al., 2019). The involvement of YTHDC1 in splicing has been associated with the incorrect processing of BRCA2, and YTHDC2 was found to contribute to metastasis (Hirschfeld et al., 2014; Tanabe et al., 2016). Additionally, YTHDF2 is a potential therapeutic target in acute myeloid leukaemia treatment (Mapperley et al., 2021). Understanding the molecular mechanisms of Pho92 in translation and decay in yeast may therefore reveal novel insights into human health and disease pathogenesis.

Acknowledgements

We are grateful to the members of the laboratory of Folkert van Werven for fruitful discussions and critical reading of the manuscript. We thank members of Ule and Luscombe labs, specifically Julian Zagalak, Christoph Sadee, Patrick Toolan-Kerr, Igor Ruiz De Los Mozos, Paulo Gameiro, Federica Capraro, Andrew Steele and Flora Lee for sharing ideas, protocols and reagents towards the iCLIP and miCLIP experiments and analysis. We acknowledge Leon Chan, Elçin Ünal, and Martin Pool for sharing reagents and Schraga Schwartz and David Dierks for providing the m6A-seq2 data and Schraga Schwartz also for initial preliminary analysis of Gis2 iCLIP and miCLIP datasets. We are grateful to Clovis Basier for providing the protocol for the HPG assay. We thank the Crick Advanced Sequencing, Proteomics,

Metabolomics, Fermentation and Genomics Equipment Park Facilities for experimental support, specifically Phil East for helping with submission to GEO, James MacRae, Christoph Messner and Svend Kjaer for technical support. The Vermeulen lab is part of the Oncode institute, which is partly funded by the Dutch Cancer Society (KWF). This research was funded in whole, or in part, by the Wellcome Trust (FC001203, FC010110, FC001134). For the purpose of Open Access, the author has applied a CC BY public copyright licence to any Author Accepted Manuscript version arising from this submission. This work was supported by the Francis Crick Institute (FC001203, FC010110, FC001134), which receives its core funding from Cancer Research UK (FC001203, FC010110, FC001134), the UK Medical Research Council (FC001203, FC010110, FC001134), and the Wellcome Trust (FC001203, FC010110, FC001134).

Contributions

R.A.V., and F.J.v.W. conceived the project. R.A.V., T.S. and F.J.v.W., designed the experiments. R.A.V. and T.S. generated strains, developed the miCLIP and iCLIP protocols, and performed all the biochemical, microscopy and genetic experiments with help from Z.M., A.R. and V.W.C.C. C.C. developed the data analysis pipeline and software for the miCLIP and iCLIP experiments, analysed the miCLIP and iCLIP data and integrated it with additional functional genomics datasets. I.E. and T.S. developed the m6A-ELISA protocol. E.C. and T.S. developed the m6A-MS protocol, and performed and analysed the m6A-MS experiments. I.E. analysed iCLIP data for selecting transcripts for further studies in Figure 6. H.P. analysed RNA-seq data. P.F. performed and analysed the IP-MS samples under the supervision of A.P.S.

J.K. processed and analysed samples for the whole proteome-MS experiment described in Figure 5. R.R.E., performed and analysed m6A-pulldowns and dimethyl labelling MS under the supervision of M.V. R.A.V. and F.J.v.W. wrote the manuscript with input from the other authors. J.U. and N.M.L. supervised the iCLIP and miCLIP data analysis and provided funding. M.R. supervised m6A-MS and provided funding. F.J.v.W. supervised the project and provided funding.

Additional files included:

Table S1. Yeast strains

Table S2. Plasmids

Table S3. Oligos sequences

Table S4. MS pulldown data

Table S5. iCLIP and miCLIP data table

Table S6. IP-MS data table

Supplemental information

Processed RNA-seq data

References:

Agarwala, S.D., Blitzblau, H.G., Hochwagen, A., and Fink, G.R. (2012). RNA methylation by the MIS complex regulates a cell fate decision in yeast. PLoS Genet *8*, e1002732.
Bodi, Z., Bottley, A., Archer, N., May, S.T., and Fray, R.G. (2015). Yeast m6A Methylated mRNAs Are Enriched on Translating Ribosomes during Meiosis, and under Rapamycin Treatment. PLoS One *10*, e0132090.
Bodi, Z., Button, J.D., Grierson, D., and Fray, R.G. (2010). Yeast targets for mRNA methylation. Nucleic Acids Res *38*, 5327-5335.
Brar, G.A., Yassour, M., Friedman, N., Regev, A., Ingolia, N.T., and Weissman, J.S. (2012). High-resolution view of the yeast meiotic program revealed by ribosome profiling. Science *335*, 552-557.
Buschauer, R., Matsuo, Y., Sugiyama, T., Chen, Y.H., Alhusaini, N., Sweet, T., Ikeuchi, K., Cheng, J., Matsuki, Y., Nobuta, R.*, et al.* (2020). The Ccr4-Not complex monitors the translating ribosome for codon optimality. Science *368*.
Bushkin, G.G., Pincus, D., Morgan, J.T., Richardson, K., Lewis, C., Chan, S.H., Bartel, D.P., and Fink, G.R. (2019). m(6)A modification of a 3' UTR site reduces RME1 mRNA levels to promote meiosis. Nat Commun *10*, 3414.
Chan, L.Y., Mugler, C.F., Heinrich, S., Vallotton, P., and Weis, K. (2018). Non-invasive measurement of mRNA decay reveals translation initiation as the major determinant of mRNA stability. Elife *7*.
Chen, J., Tresenrider, A., Chia, M., McSwiggen, D.T., Spedale, G., Jorgensen, V., Liao, H., van Werven, F.J., and Unal, E. (2017). Kinetochore inactivation by expression of a repressive mRNA. Elife *6*.
Chia, M., Li, C., Marques, S., Pelechano, V., Luscombe, N.M., and van Werven, F.J. (2021). High-resolution analysis of cell-state transitions in yeast suggests widespread transcriptional tuning by alternative starts. Genome Biol *22*, 34.
Chia, M., and van Werven, F.J. (2016). Temporal Expression of a Master Regulator Drives Synchronous Sporulation in Budding Yeast. G3 (Bethesda) *6*, 3553-3560.
Chu, S., DeRisi, J., Eisen, M., Mulholland, J., Botstein, D., Brown, P.O., and Herskowitz, I. (1998). The transcriptional program of sporulation in budding yeast. Science *282*, 699-705.
Clancy, M.J., Shambaugh, M.E., Timpte, C.S., and Bokar, J.A. (2002). Induction of sporulation in Saccharomyces cerevisiae leads to the formation of N6-methyladenosine in mRNA: a potential mechanism for the activity of the IME4 gene. Nucleic Acids Res *30*, 4509-4518.
Collart, M.A. (2016). The Ccr4-Not complex is a key regulator of eukaryotic gene expression. Wiley Interdiscip Rev RNA *7*, 438-454.
Dermody, J.L., and Buratowski, S. (2010). Leo1 subunit of the yeast paf1 complex binds RNA and contributes to complex recruitment. J Biol Chem *285*, 33671-33679.
Dierks, D., Garcia-Campos, M.A., Uzonyi, A., Safra, M., Edelheit, S., Rossi, A., Sideri, T., Varier, R.A., Brandis, A., Stelzer, Y.*, et al.* (2021). Multiplexed profiling facilitates robust m6A quantification at site, gene and sample resolution. Nat Methods *18*, 1060-1067.
Dominissini, D., Moshitch-Moshkovitz, S., Schwartz, S., Salmon-Divon, M., Ungar, L., Osenberg, S., Cesarkas, K., Jacob-Hirsch, J., Amariglio, N., Kupiec, M.*, et al.* (2012). Topology of the human and mouse m6A RNA methylomes revealed by m6A-seq. Nature *485*, 201-206.
Du, H., Zhao, Y., He, J., Zhang, Y., Xi, H., Liu, M., Ma, J., and Wu, L. (2016). YTHDF2 destabilizes m(6)A-containing RNA through direct recruitment of the CCR4-NOT deadenylase complex. Nat Commun *7*, 12626.
Duttler, S., Pechmann, S., and Frydman, J. (2013). Principles of cotranslational ubiquitination and quality control at the ribosome. Mol Cell *50*, 379-393.
Edupuganti, R.R., Geiger, S., Lindeboom, R.G.H., Shi, H., Hsu, P.J., Lu, Z., Wang, S.Y., Baltissen, M.P.A., Jansen, P., Rossa, M.*, et al.* (2017). N(6)-methyladenosine (m(6)A) recruits and repels proteins to regulate mRNA homeostasis. Nat Struct Mol Biol *24*, 870-878.
Fischl, H., Howe, F.S., Furger, A., and Mellor, J. (2017). Paf1 Has Distinct Roles in Transcription Elongation and Differential Transcript Fate. Mol Cell *65*, 685-698 e688.

Garcia-Campos, M.A., Edelheit, S., Toth, U., Safra, M., Shachar, R., Viukov, S., Winkler, R., Nir, R., Lasman, L., Brandis, A.*, et al.* (2019). Deciphering the "m(6)A Code" via Antibody-Independent Quantitative Profiling. Cell *178*, 731-747 e716.
Han, D., Liu, J., Chen, C., Dong, L., Liu, Y., Chang, R., Huang, X., Liu, Y., Wang, J., Dougherty, U.*, et al.* (2019). Anti-tumour immunity controlled through mRNA m(6)A methylation and YTHDF1 in dendritic cells. Nature *566*, 270-274.
Harigaya, Y., Tanaka, H., Yamanaka, S., Tanaka, K., Watanabe, Y., Tsutsumi, C., Chikashige, Y., Hiraoka, Y., Yamashita, A., and Yamamoto, M. (2006). Selective elimination of messenger RNA prevents an incidence of untimely meiosis. Nature *442*, 45-50.
Hirschfeld, M., Zhang, B., Jaeger, M., Stamm, S., Erbes, T., Mayer, S., Tong, X., and Stickeler, E. (2014). Hypoxia-dependent mRNA expression pattern of splicing factor YT521 and its impact on oncological important target gene expression. Mol Carcinog *53*, 883-892.
Hongay, C.F., Grisafi, P.L., Galitski, T., and Fink, G.R. (2006). Antisense transcription controls cell fate in Saccharomyces cerevisiae. Cell *127*, 735-745.
Hsu, P.J., Zhu, Y., Ma, H., Guo, Y., Shi, X., Liu, Y., Qi, M., Lu, Z., Shi, H., Wang, J.*, et al.* (2017). Ythdc2 is an N(6)-methyladenosine binding protein that regulates mammalian spermatogenesis. Cell Res *27*, 1115-1127.
Huang, H., Weng, H., Zhou, K., Wu, T., Zhao, B.S., Sun, M., Jiang, X., Wu, X., Sun, M., Guan, J.-l.*, et al.* (2019). Histone H3 trimethylation at lysine 36 guides m6A RNA modification co-transcriptionally. Nature *567*, 414-419.
Inada, T. (2020). Quality controls induced by aberrant translation. Nucleic Acids Res *48*, 1084-1096.
Ivanova, I., Much, C., Di Giacomo, M., Azzi, C., Morgan, M., Moreira, P.N., Monahan, J., Carrieri, C., Enright, A.J., and O'Carroll, D. (2017). The RNA m(6)A Reader YTHDF2 Is Essential for the Post-transcriptional Regulation of the Maternal Transcriptome and Oocyte Competence. Mol Cell *67*, 1059-1067 e1054.
Kang, H.J., Jeong, S.J., Kim, K.N., Baek, I.J., Chang, M., Kang, C.M., Park, Y.S., and Yun, C.W. (2014). A novel protein, Pho92, has a conserved YTH domain and regulates phosphate metabolism by decreasing the mRNA stability of PHO4 in Saccharomyces cerevisiae. Biochem J *457*, 391-400.
Kassir, Y., Granot, D., and Simchen, G. (1988). IME1, a positive regulator gene of meiosis in S. cerevisiae. Cell *52*, 853-862.
Ke, S., Pandya-Jones, A., Saito, Y., Fak, J.J., Vagbo, C.B., Geula, S., Hanna, J.H., Black, D.L., Darnell, J.E., Jr., and Darnell, R.B. (2017). m(6)A mRNA modifications are deposited in nascent pre-mRNA and are not required for splicing but do specify cytoplasmic turnover. Genes Dev *31*, 990-1006.
Kilchert, C., Wittmann, S., Passoni, M., Shah, S., Granneman, S., and Vasiljeva, L. (2015). Regulation of mRNA Levels by Decay-Promoting Introns that Recruit the Exosome Specificity Factor Mmi1. Cell Rep *13*, 2504-2515.
Kretschmer, J., Rao, H., Hackert, P., Sloan, K.E., Hobartner, C., and Bohnsack, M.T. (2018). The m(6)A reader protein YTHDC2 interacts with the small ribosomal subunit and the 5'-3' exoribonuclease XRN1. RNA *24*, 1339-1350.
Lasman, L., Krupalnik, V., Viukov, S., Mor, N., Aguilera-Castrejon, A., Schneir, D., Bayerl, J., Mizrahi, O., Peles, S., Tawil, S.*, et al.* (2020). Context-dependent functional compensation between Ythdf m(6)A reader proteins. Genes Dev *34*, 1373-1391.
Lee, F.C.Y., Chakrabarti, A.M., Hänel, H., Monzón-Casanova, E., Hallegger, M., Militti, C., Capraro, F., Sadée, C., Toolan-Kerr, P., Wilkins, O.*, et al.* (2021). An improved iCLIP protocol. bioRxiv, 2021.2008.2027.457890.
Lee, F.C.Y., and Ule, J. (2018). Advances in CLIP Technologies for Studies of Protein-RNA Interactions. Mol Cell *69*, 354-369.
Leger, A., Amaral, P.P., Pandolfini, L., Capitanchik, C., Capraro, F., Miano, V., Migliori, V., Toolan-Kerr, P., Sideri, T., Enright, A.J.*, et al.* (2021). RNA modifications detection by comparative Nanopore direct RNA sequencing. Nat Commun *12*, 7198.

Li, A., Chen, Y.S., Ping, X.L., Yang, X., Xiao, W., Yang, Y., Sun, H.Y., Zhu, Q., Baidya, P., Wang, X.*, et al.* (2017). Cytoplasmic m(6)A reader YTHDF3 promotes mRNA translation. Cell Res *27*, 444-447.
Linder, B., Grozhik, A.V., Olarerin-George, A.O., Meydan, C., Mason, C.E., and Jaffrey, S.R. (2015). Single-nucleotide-resolution mapping of m6A and m6Am throughout the transcriptome. Nat Methods *12*, 767-772.
Liu, J., Dou, X., Chen, C., Chen, C., Liu, C., Xu, M.M., Zhao, S., Shen, B., Gao, Y., Han, D.*, et al.* (2020). N (6)-methyladenosine of chromosome-associated regulatory RNA regulates chromatin state and transcription. Science *367*, 580-586.
Liu, J., Yue, Y., Han, D., Wang, X., Fu, Y., Zhang, L., Jia, G., Yu, M., Lu, Z., Deng, X.*, et al.* (2014). A METTL3-METTL14 complex mediates mammalian nuclear RNA N6-adenosine methylation. Nat Chem Biol *10*, 93-95.
Mao, Y., Dong, L., Liu, X.M., Guo, J., Ma, H., Shen, B., and Qian, S.B. (2019). m(6)A in mRNA coding regions promotes translation via the RNA helicase-containing YTHDC2. Nat Commun *10*, 5332.
Mapperley, C., van de Lagemaat, L.N., Lawson, H., Tavosanis, A., Paris, J., Campos, J., Wotherspoon, D., Durko, J., Sarapuu, A., Choe, J.*, et al.* (2021). The mRNA m6A reader YTHDF2 suppresses proinflammatory pathways and sustains hematopoietic stem cell function. J Exp Med *218*.
Meyer, K.D., Saletore, Y., Zumbo, P., Elemento, O., Mason, C.E., and Jaffrey, S.R. (2012). Comprehensive analysis of mRNA methylation reveals enrichment in 3' UTRs and near stop codons. Cell *149*, 1635-1646.
Neiman, A.M. (2011). Sporulation in the budding yeast Saccharomyces cerevisiae. Genetics *189*, 737-765.
Patil, D.P., Pickering, B.F., and Jaffrey, S.R. (2018). Reading m(6)A in the Transcriptome: m(6)A-Binding Proteins. Trends Cell Biol *28*, 113-127.
Pelechano, V., Wei, W., and Steinmetz, L.M. (2015). Widespread Co-translational RNA Decay Reveals Ribosome Dynamics. Cell *161*, 1400-1412.
Presnyak, V., Alhusaini, N., Chen, Y.H., Martin, S., Morris, N., Kline, N., Olson, S., Weinberg, D., Baker, K.E., Graveley, B.R.*, et al.* (2015). Codon optimality is a major determinant of mRNA stability. Cell *160*, 1111-1124.
Rojas, M., Farr, G.W., Fernandez, C.F., Lauden, L., McCormack, J.C., and Wolin, S.L. (2012). Yeast Gis2 and its human ortholog CNBP are novel components of stress-induced RNP granules. PLoS One *7*, e52824.
Rondon, A.G., Gallardo, M., Garcia-Rubio, M., and Aguilera, A. (2004). Molecular evidence indicating that the yeast PAF complex is required for transcription elongation. EMBO Rep *5*, 47-53.
Roundtree, I.A., Evans, M.E., Pan, T., and He, C. (2017). Dynamic RNA Modifications in Gene Expression Regulation. Cell *169*, 1187-1200.
Schwartz, S., Agarwala, S.D., Mumbach, M.R., Jovanovic, M., Mertins, P., Shishkin, A., Tabach, Y., Mikkelsen, T.S., Satija, R., Ruvkun, G.*, et al.* (2013). High-resolution mapping reveals a conserved, widespread, dynamic mRNA methylation program in yeast meiosis. Cell *155*, 1409-1421.
Shah, J.C., and Clancy, M.J. (1992). IME4, a gene that mediates MAT and nutritional control of meiosis in Saccharomyces cerevisiae. Mol Cell Biol *12*, 1078-1086.
Shahbabian, K., Jeronimo, C., Forget, A., Robert, F., and Chartrand, P. (2014). Co-transcriptional recruitment of Puf6 by She2 couples translational repression to mRNA localization. Nucleic Acids Res *42*, 8692-8704.
Shichino, Y., Otsubo, Y., Kimori, Y., Yamamoto, M., and Yamashita, A. (2018). YTH-RNA-binding protein prevents deleterious expression of meiotic proteins by tethering their mRNAs to nuclear foci. Elife *7*.
Steber, C.M., and Esposito, R.E. (1995). UME6 is a central component of a developmental regulatory switch controlling meiosis-specific gene expression. Proc Natl Acad Sci U S A *92*, 12490-12494.
Tanabe, A., Tanikawa, K., Tsunetomi, M., Takai, K., Ikeda, H., Konno, J., Torigoe, T., Maeda, H., Kutomi, G., Okita, K.*, et al.* (2016). RNA helicase YTHDC2 promotes cancer metastasis via the enhancement of the efficiency by which HIF-1alpha mRNA is translated. Cancer Lett *376*, 34-42.

Trcek, T., Larson, D.R., Moldon, A., Query, C.C., and Singer, R.H. (2011). Single-molecule mRNA decay measurements reveal promoter- regulated mRNA stability in yeast. Cell *147*, 1484-1497.
Van Oss, S.B., Cucinotta, C.E., and Arndt, K.M. (2017). Emerging Insights into the Roles of the Paf1 Complex in Gene Regulation. Trends Biochem Sci *42*, 788-798.
van Werven, F.J., and Amon, A. (2011). Regulation of entry into gametogenesis. Philos Trans R Soc Lond B Biol Sci *366*, 3521-3531.
Viphakone, N., Sudbery, I., Griffith, L., Heath, C.G., Sims, D., and Wilson, S.A. (2019). Co-transcriptional Loading of RNA Export Factors Shapes the Human Transcriptome. Mol Cell *75*, 310-323 e318.
Wang, C., Zhu, Y., Bao, H., Jiang, Y., Xu, C., Wu, J., and Shi, Y. (2016). A novel RNA-binding mode of the YTH domain reveals the mechanism for recognition of determinant of selective removal by Mmi1. Nucleic Acids Res *44*, 969-982.
Wang, X., Lu, Z., Gomez, A., Hon, G.C., Yue, Y., Han, D., Fu, Y., Parisien, M., Dai, Q., Jia, G*., et al.* (2014). N6-methyladenosine-dependent regulation of messenger RNA stability. Nature *505*, 117-120.
Wang, X., Zhao, B.S., Roundtree, I.A., Lu, Z., Han, D., Ma, H., Weng, X., Chen, K., Shi, H., and He, C. (2015). N(6)-methyladenosine Modulates Messenger RNA Translation Efficiency. Cell *161*, 1388-1399.
Xiao, W., Adhikari, S., Dahal, U., Chen, Y.-S., Hao, Y.-J., Sun, B.-F., Sun, H.-Y., Li, A., Ping, X.-L., Lai, W.-Y*., et al.* (2016). Nuclear m6A Reader YTHDC1 Regulates mRNA Splicing. Molecular Cell *61*, 507-517.
Xu, C., Liu, K., Ahmed, H., Loppnau, P., Schapira, M., and Min, J. (2015). Structural Basis for the Discriminative Recognition of N6-Methyladenosine RNA by the Human YT521-B Homology Domain Family of Proteins. J Biol Chem *290*, 24902-24913.
Yang, C., Hu, Y., Zhou, B., Bao, Y., Li, Z., Gong, C., Yang, H., Wang, S., and Xiao, Y. (2020). The role of m(6)A modification in physiology and disease. Cell Death Dis *11*, 960.
Zaccara, S., and Jaffrey, S.R. (2020). A Unified Model for the Function of YTHDF Proteins in Regulating m(6)A-Modified mRNA. Cell *181*, 1582-1595 e1518.
Zaccara, S., Ries, R.J., and Jaffrey, S.R. (2019). Reading, writing and erasing mRNA methylation. Nat Rev Mol Cell Biol *20*, 608-624.
Zhou, J., Wan, J., Gao, X., Zhang, X., Jaffrey, S.R., and Qian, S.B. (2015). Dynamic m6A mRNA methylation directs translational control of heat shock response. Nature *526*, 591-594.

Figure legends

Figure 1. Pho92, but not Gis2, binds to m6A modified transcripts.

(**A**) Schematic overview of the yeast meiotic program. Ime1 induces the transcription of the MIS complex. m6A occurs during early meiosis. (**B**) Scheme describing set up for synchronized meiosis. Cells were grown in rich medium till saturation, shifted to SPO, and cells were induced to enter meiosis using *CUP1* promoter fused to *IME1* (*pCUP-IME1*, FW2444). Time points were taken at 2h and 4h. (**C**) Scatter plot displaying proteins identified in m6A consensus oligo pull down versus control. In short, cells were grown in rich medium till saturation, and shifted to SPO, and cells were induced to enter meiosis using *CUP1* promoter fused to *IME1* (*pCUP-IME1*, FW 2444). Protein extracts were incubated using m6A and control RNA oligo bound to streptavidin beads. Eluted proteins were differentially labelled with light and heavy dimethyl isotopes, mixed, and proteins from forward and reverse label swap reactions were identified by MS. (**D**) *In vitro* m6A pull down to assess binding of GST-Pho92 and GST-Gis2. Expression of GST-Pho92 and GST-Gis2 were induced in bacteria, clarified lysates were incubated with m6A consensus and control RNA oligos bound to streptavidin beads, and eluates were run on an SDS-page gel and Coomassie-stained. Input (IN), Unlabelled oligo (C), m6A oligo (m6A), Unbound flow through after incubation (FT). (**E**) Similar as D except that lysates from truncations of GST-Pho92 in N-terminus (NΔ) and YTH domain (YTHΔ) were used. (**F**) Pho92 expression prior to and during meiosis. Cells harbouring *pCUP-IME1* and Pho92 tagged with V5 (FW 9962) were induced to enter meiosis in sporulation medium

(SPO). After 2 hours in SPO, Ime1 was induced with copper sulphate (labelled with *). Samples were taken at the indicated time points, and RNA and protein levels were determined by RT-qPCR and western blotting. *ACT1* and Hxk1 was used for normalization or loading control respectively. (**G**) ChIP-seq data for Ume6 at the *PHO92* locus. Indicated are the Ume6 binding site, and the ChIP-seq signal. Data were taken from *Chia* et al (2021). (**H**) Experimental setup for Pho92 4TU-iCLIP, Gis2 iCLIP, and m6A CLIP (miCLIP) in wild-type (WT) and *ime4*Δ cells. (**I**) Integrative genome browser (IGV) view of *BDF2* gene for Pho92, Gis2 iCLIP and miCLIP in WT and *ime4*Δ cells. Tracks are crosslink per million normalised, strand-specific bigWigs. (**J-L**) Volcano plots comparing WT and *ime4*Δ cells for miCLIP (J), Gis2 iCLIP (K), and Pho92 4TU-iCLIP (L). The Ime4-dependent binding sites are labelled, as determined by a criteria of log2FoldChange <= -1 and adjusted p value < 0.001 for miCLIP and log2FoldChange <= -2 and adjusted *p*-value < 0.001 for the two iCLIP experiments. (**M**) Metanalysis comparing the miCLIP-identified m6A sites to a compendium of published m6A data. For each m6A site the closest published m6A site was calculated. (**N**) Similar as M except that Pho92 binding sites that depended on Ime4 were compared to m6A sites (miCLIP). (**O**) Similar as M except that Gis2 Ime4 dependent sites were compared to m6A sites (miCLIP).

Figure S1. Pho92, but not Gis2, binds to m6A marked transcripts *in vitro* and *in vivo*.

(**A**) Scheme describing setup for pull-down experiment. In short, protein extracts were incubated using m6A and control RNA oligo bound to streptavidin beads. Eluted proteins were labelled with heavy (H) and light (L) dimethyl isotopes, mixed, and proteins were identified by MS. (**B**) Scatter plots displaying proteins identified in

m6A oligo pull down versus control in pre-meiosis (PM). (**C**) Gis2 does not bind to m6A labelled or unlabelled oligos but does to control RNA oligos. Protein extracts expressing Gis2-V5 (FW 3312) were incubated with unlabelled oligo, m6A oligo, and control oligo harbouring the canonical Gis2 motif (GA(A/U)). (**D**) Pho92 expression prior and during meiosis. Diploid cells with Pho92 tagged with V5 (FW 4478) were induced to enter meiosis in sporulation medium (SPO). Samples were taken at the indicated time points, and Pho92 RNA and protein levels were determined by RT-qPCR and western blotting. (**E**) Principle component analysis (PCA) of miCLIP (left), Pho92 iCLIP (middle), and Gis2 iCLIP (right) at the level of counts per peak. Indicated are the biological repeats for the WT (blue) and *ime4*Δ (yellow). (**F**) Autoradiograph showing the protein RNA complexes in control untagged (C) and Pho92-V5 cells. In short, cells were grown till 4 hours in SPO in presence of 4-thiouracil. Cell were harvested and either crosslinked or left untreated. Protein extracts were generated, and Pho92 was immunoprecipitated with anti V5 antibodies. RNA-protein complexes were labelled with (γ-^{32}P)-ATP, and separated by SDS page, and transferred to nitrocellulose membrane. Displayed are the signals obtained for untagged control (FW 4256), Pho92-V5 (WT, FW 4472), and Pho92-V5 in *ime4*Δ (FW 4505). In right panel, western blots probed with anti-V5 showing the immunoprecipitation of Pho92. (**G**) Integrative genome browser (IGV) tracks of *NDC80* gene for Pho92 CLIP in WT and *ime4*Δ, and untagged control CLIP in WT background. Tracks are crosslink per million normalised, strand-specific bigWigs. (**H**) A Venn diagram showing the number of miCLIP and published m6A sites within 100nt of each other. (**I**) Metanalysis comparing the distance between Ime4-dependent Pho92 binding sites to curated m6A sites from published datasets. For each Pho92 binding site the distance to the nearest m6A site was calculated. (**J**)

Similar as I except that Gis2 Ime4 dependent sites were compared to the curated m6A sites. (**K**) Metagene analysis of Pho92 CLIP Ime4 dependent sites for WT and *ime4*Δ cells. Data was centred on the m6A sites identified with miCLIP.

Figure 2. Features of transcripts bound by Pho92

(**A**) *IME1* and *RIM4* transcripts bound by Ime4-dependent Pho92. Shown are the crosslinks per million normalised bigWigs for Pho92 iCLIP and miCLIP in WT and *ime4*Δ cells. Underlined are the binding sites identified in the analysis. (**B**) Similar as A, except that *IME2* locus is displayed, which exhibits an m6A peak but no Pho92 binding. The m6A site is labelled. * this was reported in our analysis below the significance threshold (log2FC=-0.6, padj= 0.007). (**C**) Venn diagram showing the overlap between genes with m6A sites and Ime4-dependent Pho92 binding. (**D**) Sequence logos of the top ranked motifs from m6A sites and Ime4-dependent Pho92 sites as determined by STREME. (**E**) Pho92 metagene profile split into genes containing Ime4-dependent Pho92 binding sites (left) and Ime4-independent sites (right). The matrix underlying the heatmap is scored 1 for binding site and 0 for no binding, intermediate values between 0 and 1 are due to smoothing in the visualisation. (**F**) Number of m6A sites (miCLIP) per transcript. On the x-axis transcripts with 1, 2, 3, 4 or 5 bindings sites. On the y-axis the number of genes for each category is displayed. (**G**) Similar to F, except that Pho92 binding sites were analysed. (**H**) Motif enrichment around m6A sites and Pho92 Ime4-dependent and independent binding sites for RGAC. Motif frequency plotted around the centre of Pho92 binding sites, split into Ime4-dependent sites (solid line) and Ime4-independent sites (dotted line). (**I**) Gene ontology (GO) enrichment analysis for Pho92 bound transcripts (left) and m6A harbouring transcripts based on the miCLIP

analysis (right). On the y-axis the category of processes involved, while on x-axis the -log10(adjusted *P*-value) is displayed. (**J**) *HOP1, MEI5, and SPO24* transcripts bound by Pho92 and marked with m6A. Data tracks are crosslinks per million normalised bigWigs, visualised in IGV. Underlined are the binding sites identified in the analysis. * this was reported in our analysis below the significance threshold (log2FC=-0.94, padj= 0.004).

Figure S2. Features of transcripts bound by Pho92

(A) *IME1* and *HOP1* IGV tracks. Shown are the crosslinks per million normalised bigWigs for Pho92 iCLIP, and miCLIP in WT and *ime4*Δ cells. Underlined are the binding sites identified in the analysis. * this site was reported in our analysis below the significance threshold (miCLIP). The bottom IGV track shows the significant m6A sites identified with comparative Nanopore direct RNA sequencing, with the scale of the bars representing -log10(p value) from a logistic regression test, (Nanocompore, WT versus *ime4*Δ) (Leger *et al*, 2021). **(B)** Motif analysis of Ime4-dependent Pho92 binding sites, m6A sites (miCLIP) and Ime4-independent Pho92 binding sites using STREME. Significant motif sequences are shown. **(C)** Motif enrichment around m6A sites and Pho92 Ime4-dependent and independent binding sites for RGAC and ANNRGACNNU motifs. Motif frequency plotted around the centre of Pho92 binding sites, split into Ime4-dependent sites (solid line) and Ime4-independent sites (dotted line). (**D**) Stacked bar graph showing peak distributions over transcript regions for m6A sites, and Pho92 Ime4-dependent and independent binding sites.

Figure 3. Pho92 is important for meiosis and fitness of gametes

(**A**) Venn diagram displaying the comparison between RNA-seq of *ime1*Δ (FW81) and *ndt80*Δ (FW 4911), and transcripts bound by Pho92. For this analysis, Ime1 and Ndt80-dependent genes were selected by taking the transcripts that were significantly down-regulated compared to the WT control. (**B**) Onset of meiosis in WT, *pho92*Δ, and *ime4*Δ cells (FW1511, FW3528, and FW725). Cells were grown in rich medium till saturation, shifted to pre-sporulation medium and grown for an additional 16 hours. Subsequently, cells were shifted to SPO, and samples were taken at the indicated time points. Cells were fixed, and stained, DAPI masses were counted for at least n=200 cells per biological repeat. The error bar represents the standard error of the mean of n=3 experiments. Cells with two or more DAPI masses were considered as undergoing meiosis. (**C**) Similar as B, except that cells were induced to undergo meiosis using *pCUP-IME1* (WT FW2444, *pho92*Δ FW3576). Cells were grown as described in B, shifted to SPO, and after 2 hours treated with copper sulphate to induce *IME1* expression. (**D**) Similar as C, except that these also harboured *NDT80* under control of the *GAL1-10* promoter and fused Gal4 activation domain plus estrogen receptor (Gal4ER). Ndt80 expression was induced at 2 hours in SPO with β-estradiol together with Ime1 expression (WT FW2795, *pho92*Δ FW9070). (**E**) Similar as B, except that S288C strain background was used for the analysis (WT FW631, *pho92*Δ FW8983, *ime4*Δ FW8985). (**F**) Similar analysis as B, except that A364A was used for the analysis (WT FW1671, *pho92*Δ FW8912, *ime4*Δ FW8913). (**G**) Spore packaging was assessed in WT and *pho92*Δ strains (S288C and A364A strains as in E and F). Number of packaged spores per ascus were counted for at least 200 asci. (**H**) Spore viability of WT (FW 1511) and *pho92*Δ (FW3531). Cells were patched from YPD agar plates to SPO agar plates and incubated for 3 days at 30°C or 37°C. Subsequently tetrads were dissected, and

spores grown on YPD agar plates. The fraction of viable and not viable spores are indicated. At least n=150 spores for each condition (30°C or 37°C) and each strain (WT and *pho92*Δ) were used for the analysis.

Figure S3. Pho92 is important for meiosis and fitness of gametes

Venn diagram displaying the comparison between RNA-seq of *ime1*Δ (FW81) and *ndt80*Δ (FW4911), and transcripts determined by miCLIP. For this analysis, Ime1 and Ndt80-dependent genes were selected by taking the transcripts that were significantly down-regulated compared to the WT control in the *ime1*Δ and *ndt80*Δ.

Figure 4. Paf1C interacts with Pho92 to direct Pho92 to nucleus

(**A**) Volcano plot IP-MS of Pho92 (left). Cells expressing the *CYC1* promoter (*pCYC1*-FLAG-Pho92, FW8734) controlling Pho92 expression and a FLAG-tag at the amino terminus were grown in rich medium conditions. Cell extracts from *pCYC1*-FLAG-Pho92 and control (FW629) were incubated with anti-FLAG beads and eluted with FLAG peptides and analysed by MS using label free quantification method. Significantly enriched proteins are displayed in red. Table (right) proteins enriched in IP-MS experiments (also data from plots in S4). Highlighted are the processes and protein complexes enriched. (**B**) Co-immunoprecipitation of Pho92 and Paf1C. We used strains where *pPYK1*-FLAG-Pho92 was expressed with or without tagged HA-Paf1 or HA-Leo1 (FW9880 and FW9791). Cells harbouring FLAG-Pho92, HA-Paf1, or HA-Leo1 only were used as control (FW8732, FW9782 and FW9763). As a negative, control membranes were also probed for Hxk1, which does not interact with Pho92. (**C**) Pull-down of Paf1C by GST-Pho92, GST-Gis2 or GST alone induced in bacteria. Cell extracts were prepared and immobilized on

Glutathione- agarose beads. GST-Pho92 bound to beads were subsequently incubated with extracts expressing HA-tagged Paf1, Leo1, Crt9, and Rap1 (FW9782, FW9763, FW9784, FW 4948). (**D**) Localization of Pho92 during entry in meiosis. Cells expressing Pho92 fused with mNeongreen (Pho92-mNG, FW9633) were used for the analysis. To determine nuclear localization, we used histone H2B fused to mCherry (H2B-mCh) and the cells also harboured *pCUP-IME1* to enable induction of synchronous meiosis. Cells were treated with copper sulphate at 2 hours (labelled with *), and samples were taken at the indicated time points. (**E**) Quantification of nuclear over cytoplasmic signal for Pho92-mNG in WT and *leo1*Δ (FW9633 and FW9736). Cells were grown as described in D. At least 150 cells were quantified per time point. Each datapoint is shown in addition to the box plots. ** $P< 0.01$ Welch's paired t test. (**F**) Similar to E, except with Paf1 depletion strain. Paf1 is fused to an auxin induced degron (AID-tag), which is induced by copper sulphate and IAA treatment at 2h (FW10128). These cells also express *TIR1* ligase under control of the *CUP1* promoter. Cells harbouring the *TIR1* ligase alone were used as controls (FW10129). (**G**) Same as in E, except that *ime4*Δ cells were used for the analysis (FW9604). (**H**) Pho92 binding overlaps with *BMH2* and *DMC1* introns. Data tracks of Pho92 iCLIP, miCLIP, and miCLIP-input in WT and *ime4*Δ cells. Intron regions are designated with dashed lines. (**I**) ChIP-qPCR of Pho92 at the *BDF2* and *GUT2* loci during entry into meiosis in WT (FW4478) and *leo1*Δ (FW10113) cells. Biological repeats of WT and *leo1*Δ cells were grown in parallel, each sample was input normalized, subsequently the primer pair with highest signal was set to 1 for each biological repeat, which was primer pair p4 for 3h WT *BDF2* and *GUT2*. The relative mean signal of n=2 biological repeats are displayed.

Figure S4. Paf1C interacts with Pho92 to direct Pho92 to nucleus

(**A**) Western blot of Pho92 eluates used for MS analysis. Diploid cells harbouring Pho92-V5 tagged and untagged control (FW4478 and FW1511). Cells were grown and induced to enter meiosis, and samples were collected at 4h in SPO. Cell extracts were incubated with anti-V5 beads and eluted with V5 peptides followed by laemmli sample buffer boiling elution. E1, E2 and E3 represent peptide eluates. (**B**) Similar as A, except that cells with the *PYK1* or *CYC1* promoter (*pPYK1*-FLAG-Pho92, FW8732; *pCYC1*-FLAG-Pho92, FW8734) controlling Pho92 expression and a FLAG-tag at the amino terminus were grown in rich medium conditions. Cell extracts were incubated with anti-FLAG beads and eluted with FLAG peptides. E1, E2 and E3 represent eluates. **(C)** Volcano plots of IP-MS of Pho92-V5 compared to untagged control. Significantly enriched proteins are displayed in red. Pho92 is labelled in black. (**D**) Volcano plots of IP-MS of Pho92 *pPYK1*-FLAG-Pho92 compared to untagged control. (**E**) Whole cell quantification of Pho92-mNG in WT and *leo1*Δ cells during entry into meiosis. These cells also harboured *pCUP-IME1*. Cells were treated with copper sulphate at 2 hours. Samples were taken at the indicated time points. Signal for Pho92-mNG in WT and *leo1*Δ (FW9633 and FW9736). At least 150 cells were quantified per time point. (**F**) Similar as E, except that Paf1 depletion allele was used for the analysis. Paf1 fused to the auxin induced degron (AID) was used (FW10128). These cells expressed *TIR1* ligase under control of the *CUP1* promoter. The depletion was induced by treating cells with copper sulphate and IAA. Cells harbouring the *TIR1* ligase alone were used as controls (FW10129). (**G**) Same as in E, except that *ime4*Δ cells (FW9604) were used for the analysis. **(H)** Western blot of strains used in F showing the depletion of *PAF1-AID*. * indicates treatment with copper sulphate and IAA. (**I**) Pho92 binds to some intronic

regions in transcripts. IGV data tracks of Pho92 CLIP, miCLIP, and input in WT and *ime4*Δ cells. Intron regions of *BMH2* and *DMC1* are shown. (**J**) Pho92 expression in WT and *leo1*Δ cells during entry into meiosis. Diploid cells harbouring Pho92-V5 in WT and *leo1*Δ (FW4478 and FW10113) were induced to enter meiosis. Samples were taken at the indicated time points, and protein extracts were assessed by western blotting with anti-V5 antibodies. As a loading control Hxk1 was used. (**K**) Onset of meiosis in WT and *leo1*Δ cells (FW4478 and FW10113). Cells were shifted to SPO, and samples were taken at the indicated time points. Cells were fixed, and stained, DAPI masses were counted for at least n=200 cells per biological repeat. Cells with two or more DAPI masses were considered as undergoing meiosis. (**L**) m6A ELISA during entry into meiosis of WT, *ime4*Δ and *leo1*Δ cells (left) and after Paf1 depletion as described in F (right). The relative m6A signals are displayed.

Figure 5. Pho92 interacts with polysomes and controls protein expression

(A) Sucrose cushion analysis of cells expressing *pPYK1*-FLAG-Pho92 (FW 8732) were grown in rich medium. Immunoblots of total (T), pellet/ribosomal (P) and soluble (S) fractions are shown for FLAG-Pho92, hexokinase (Hxk1) and Rpl35 (ribosomal subunit of 60S) proteins. (**B**) Polysome fractionation and western blot of Pho92. Diploid cells harbouring Pho92 tagged with V5 (FW4478). Cells were induced to enter meiosis and at 4 hours in SPO samples were taken. The small (40S), large (60S), both (80S) subunits and polysomes are highlighted from the polysome traces. Protein extracts from fractions were probed for Pho92-V5 by immunoblotting. As controls membranes were probed for Rpl35 and Hxk1. (**C**) Ribosome footprint and mRNA-seq (RPKM) data from Brar et al (2012) at the *BDF2* locus. *BDF2* has multiple m6A peaks and Pho92 binding sites. Indicated are the

different phases of yeast gametogenesis. (**D**) Analysis of translation efficiency (TE) using Brar et al 2012 dataset. We assessed the TE for transcripts harbouring Ime4-dependent Pho92 binding sites, m6A sites and a control set of transcripts comprised of the rest of expressed mRNAs at 4h in SPO. Boxes show the median and interquartile range, extending lines show first and fourth quartiles. (**E**) Same as D, except TE was assessed for Pho92 bound transcripts either with either one or multiple binding sites (as categorised in Figure 2G) (**F**) Monosome over Polysome ratio for WT (FW1511), *pho92*Δ (FW3528), and *ime4*Δ (FW725). Cells were induced to enter meiosis, samples were taken at 4 hours in SPO. From the polysome traces we determined the ratio of monosomes over polysomes. Signals for n=3 biological repeats are displayed. (**G**) HPG assay for WT (FW1511) and *pho92*Δ (FW3528) cells. Cells were treated with Click-iT homopropargylglycine (HPG) for 30 min at 4 hours in SPO, labelled, and fluorescent signals were measured. As a control cells were also treated with cycloheximide (+CHX). At least n=50 cells were quantified. (**H**) Similar assay described in A, except that WT and *pho92*Δ cells were used for the analysis, and the membrane was probed with α-ubiquitin antibodies. (**I**) Violin plots describing RNA-seq and proteome data from comparing *pho92*Δ to control. In short, cells were induced to enter meiosis. Samples for RNA-seq and whole proteome analysis were taken at 4 hours in SPO for WT (FW1511) and *pho92*Δ (FW3528) cells. Transcripts showing binding of Pho92 by CLIP and with a signal in whole proteome quantification were used for the analysis. The RNA-seq data divided in the three groups (1 to 3), while group 1 represents genes with the reduced RNA-seq signal, group 2 little change, group 3 upregulated in *pho92*Δ RNA-seq. The corresponding protein signal from the whole proteome analysis is displayed. (**J**)

Similar analysis as I, except that the control entailed a group of genes up-regulated in the RNA-seq that were not bound by Pho92 were used for the analysis.

Figure S5. Pho92 interacts with polysomes and controls protein expression

(A) Sucrose cushion of cells expressing *pCYC1*-FLAG-Pho92 (FW 8734). Cells were grown in rich medium. Immunoblots of total (T), pellet/ribosomal (P) and soluble (S) fractions are shown for FLAG-Pho92, hexokinase (Hxk1) and Rpl35 (ribosomal subunit of 60S) proteins. (**B**) Polysome traces from cells grown in rich medium (YPD), and cells in early meiosis (4h in SPO). (**C**) Western blot of Pho92 associates with polysomes. Haploid cells harbouring *pPYK1*-FLAG-Pho92 (FW 8732) were grown in rich medium (YPD). 80S and polysomes are highlighted from the polysome traces. Protein extracts from fractions were probed of Pho92-V5 by immunoblotting. As controls we probed membranes for Rpl35. (**D**) Ribosome footprint and mRNA-seq data from Brar et al showing *RIM4* and *GUT2* locus. Indicated are the different phases of yeast gametogenesis. (**E**) Polysome traces of cells entering meiosis (SPO 4H) for WT (FW1511), *ime4*Δ (FW5486), and *pho92*Δ (FW3528) cells. (**F**) HPG assay for WT (FW1511) and *pho92*Δ (FW3528) cells. Cells were treated with Click-iT homopropargylglycine (HPG) for 0, 10 or 30 min at 4h in SPO, labelled, and fluorescent signals were measured. At least n=50 cells were quantified. (**G**) Related to Figure 5H, except that the membrane was probed with α-Rpl35 antibodies. (**H**) Violin plots describing RNA-seq and proteome data from comparing *pho92*Δ (FW3528) to control (FW1511). In short, cells were induced to enter meiosis. Samples for RNA-seq and whole proteome analysis were taken at 4 hours in SPO for WT and *pho92*Δ cells. Transcripts with Ime4-dependent Pho92 binding sites and with a signal in whole proteome quantification were used for the

analysis. Also a control set of transcripts was used for the analysis that showed no binding to Pho92. The RNA-seq data divided in the three groups (1 to 3), while group 1 represents genes with the reduced RNA-seq signal, group 2 little change, group 3 upregulated in *pho92*Δ RNA-seq. The corresponding signal from the whole protein data is displayed.

Figure 6. Pho92 and Paf1C promote protein production of targets.

(A) *SRT1, RGT1, GUT2* and *INO1* transcripts bound by Pho92 and marked with m6A. Shown are the data tracks for Pho92 CLIP for WT (FW4472) and *ime4*Δ (FW4505) cells, and miCLIP for WT (FW1511) and *ime4*Δ (FW725). Underlined are the binding sites identified in the analysis. Tracks are crosslink per million normalised stranded bigWigs viewed in IGV. **(B)** Relative protein, RNA, and protein over RNA ratios. WT and *pho92*Δ cells were grown to enter meiosis and samples from time points indicated for protein and RNA quantification were collected (FW9949 and FW9950). For the analysis *SRT1* was tagged seamlessly with sfGFP at the amino terminus. Left panel, sfGFP-Srt1 protein expression was determined by western blotting. The relative signal is displayed with max signal for each biological repeat scaled to one. Middle panel. sfGFP-SRT1 RNA levels were determined by RT-qPCR. The relative signal was computed by setting the maximum signal for each time course experiment (which included WT and *pho92*Δ) repeat to one. Right panel. The ratio of protein and RNA signals. The relative signal was computed by setting the maximum signal for each time course experiment (which included WT and *pho92*Δ) repeat to 1. **(C)** Similar analysis as B, except that *IME2* protein over RNA signals are displayed. For the analysis *IME2* was tagged with V5 at the C-terminus (FW10450 and FW5190). **(D)** Similar analysis as C, except that *RGT1*

protein over RNA signals are displayed. For the analysis *RGT1* was tagged with V5 at the C-terminus (FW9951 and FW9952). **(E)** Similar analysis as C, except that *GUT2* protein over RNA signals are displayed. For the analysis *GUT2* was seamlessly tagged with sfGFP at the N-terminus (FW9836 and FW9781). **(F)** Similar analysis as C, except that *INO1* protein over RNA signals are displayed. For the analysis meiosis was induced using *pCUP-IME1* synchronization system. For the analysis *INO1* was seamlessly tagged with sfGFP at the N-terminus (FW9746 and FW9747). **(G)** Similar analysis as C, except that *BDF2* protein over RNA signals are displayed. For the analysis meiosis was induced using *pCUP-IME1* synchronization system. For the analysis *BDF2* was tagged with V5 at the C-terminus (FW 8973 and FW 9093). **(H)** Similar analysis as C, except that *GUT2* protein over RNA signals are displayed in the presence or absence of Pho92 expression from the *CUP1* promoter (FW 10438 and *ime4Δ*, FW10441). **(I)** Similar analysis as C, except that *IME2* protein over RNA signals are displayed in the presence or absence of Pho92 expression from the *CUP1* promoter (FW 10522). **(J)** Similar analysis as C, except that *GUT2* protein over RNA signals are displayed in WT and *leo1*D (FW 10230 and FW 10241). **(K)** Similar analysis as C, except that *BDF2* protein over RNA signals are displayed in WT and *leo1*Δ (FW8859 and FW10199).

Figure S6. Pho92 and Paf1C promote protein production of targets

(A) *IME2* protein and RNA levels. WT and *pho92*Δ cells were grown to enter meiosis and samples from indicated time points for protein and RNA quantification were taken. For the analysis *IME2* was tagged with V5 at the C-terminus (FW10450 and FW5190). Left panel, Ime2 protein expression was determined by western blot. The

relative signal is displayed with max signal for each biological repeat scaled to one. Middle panel. Ime2 protein levels. The relative signal was computed by setting the maximum signal for each time course experiment (which included WT and *pho92*Δ) repeat to one. Right panel. RNA signals. The relative signal was computed by setting the maximum signal for each time course experiment (which included WT and *pho92*Δ) repeat to one. **(B)** Similar analysis as B, except that *RGT1* protein over RNA signals are displayed (FW9951 and FW9952). **(C)** Similar analysis as C, except that Gut2 protein over RNA signals are displayed (FW9836 and FW9781). **(D)** Similar analysis as C, except that Ino1 protein over RNA signals are displayed. For the analysis meiosis was induced using *pCUP-IME1* synchronization system (FW9746 and FW9747). **(E)** Similar analysis as C, except that Bdf2 protein over RNA signals are displayed. For the analysis meiosis was induced using *pCUP-IME1* synchronization system (FW8973 and FW9093). **(F)** Similar analysis as A, except that Gut2 protein over RNA signals are displayed in the presence or absence of Pho92 expression from the Cup1 promoter (FW 10438 and *ime4Δ*, FW 10441). **(G)** Similar analysis as C, except that Ime2 protein over RNA signals are displayed in the presence or absence of Pho92 expression from the Cup1 promoter (FW 10522). **(H)** Similar analysis as C, except that Gut2 protein over RNA signals are displayed in WT and *leo1*Δ (FW 10230 and FW 10241). **(I)** Similar analysis as C, except that Bdf2 protein over RNA signals are displayed in WT and *leo1*Δ (FW8859 and FW10199).

Figure 7. Pho92 and CCR4-NOT promotes translation coupled decay of m6A marked transcripts

(A) Differential analysis of *pho92*Δ vs WT for transcripts with Ime4-dependent Pho92 binding sites. Samples were taken at 0 and 4 hours in SPO for WT and *pho92*Δ cells

(FW1511 and FW3528). RNA-seq was performed. Displayed are transcripts that are bound by Pho92 in an Ime4 dependent manner as determined by iCLIP. Differential expression between 0h in SPO for *pho92*Δ vs WT are displayed (red), and 4h in SPO *pho92*Δ vs WT are displayed (blue). **(B)** Metagene analysis plotting Ime4-dependent Pho92 binding sites on genes that were either significantly upregulated, down regulated, or unchanged in 4h in SPO *pho92*Δ vs WT RNA-Seq. The y-axis represents the proportion of transcripts in that RNA-seq category with a binding site overlapping a given x coordinate. **(C)** m6A-MS for control, *ime4*Δ, and *pho92*Δ (FW4911, FW6060, and FW6997). Samples were grown as described in A, samples were taken at 6h in SPO. mRNA was isolated using oligodT paramagnetic beads. Samples were digested, and m6A levels of A were determined by LC-MS. (**D**) Similar analysis as A, except that the RNA-seq analysis of total and polysomal bound mRNAs was performed 4h SPO *pho92*Δ vs WT. Ribosomal fractionation was performed to isolate mRNAs bound to polysomes. RNA-seq was performed in total RNA and polysome-associated RNA fractions. **(E)** Relative m6A levels in depletion mutants of various decay pathways determined by m6A-MS and m6A-seq2 (FW5958, FW6080, FW6048, FW5880, FW 6070, FW6043, FW5956, FW5964). In short, cells were grown and induced to enter meiosis. Each decay mutant bearing auxin-induced depletion alleles (AID) was depleted by adding auxin at 4h in SPO, and samples were collected at 6 hours in SPO. m6A-MS and m6A-seq2 data were normalized to a control strain harbouring the *TIR* ligase. m6A-seq2 data were obtained from Dierks et al (2021). **(F)** Similar analysis as E, except that the signals for *ime4*Δ and *not3*Δ cells are shown (control, FW4911, FW6060 and FW6093). (**G**) m6A-ELISA in WT and *pho92*Δ cells (FW1511 and FW3528) after blocking transcription using thiolutin. Cells were grown and induced to enter meiosis. Cells

were treated with thiolutin, and samples were taken at the indicated time points. Relative m6A levels were determined by m6A-ELISA. **(H)** Similar analysis as G, but cells were treated with both thiolutin and cycloheximide. (**I**) m6A-ELISA comparing WT, *pho92*Δ and *not3*Δ signal before and after blocking transcription with thiolutin for 15 min. Cells were grown to be induced to enter meiosis (FW1511, FW3528 and FW6090). Cells were treated with thiolutin, and samples were taken at 15 min after treatment. Relative m6A levels were determined by m6A-ELISA. (**J**) Model for Pho92's role in early meiosis. Pho92 and MIS complex (Ime4) expression are induced by Ime1. Subsequently, Pho92 is loaded to mRNAs during transcription via Paf1C, and Pho92 promotes the translation to decay fate of m6A modified transcripts involving CCR4-NOT.

Figure S7. Pho92 and CCR4-NOT promotes translation coupled decay of m6A marked transcripts

(A) Venn diagrams comparing differentially expressed transcripts in *pho92*Δ RNA-seq vs transcripts with Ime4-dependent Pho92 binding. (**B**) Similar as A, except that differentially expressed transcripts from *ime4*Δ vs WT RNA-seq is compared to Pho92-bound transcripts. (**C**) Differential analysis of *pho92*Δ or *ime4*Δ vs WT RNA-seq subsetted for transcripts with Ime4-dependent Pho92 binding. Differential expression between 0h (red) and 4h (blue) time points for *pho92*Δ or *ime4*Δ vs WT are displayed. (**D**) Metagene analysis plotting Ime4-dependent Pho92 binding sites on genes that were either significantly upregulated, down regulated, or unchanged in 4 hours SPO *ime4*Δ vs WT RNA-seq. The y-axis represents the proportion of transcripts in that RNA-seq category with a binding site overlapping a given x coordinate. (**E**) m6A-MS in WT and *pho92*Δ cells (FW1511 and FW 3528) after

blocking transcription using thiolutin. Cells were grown and induced to enter meiosis. Cells were treated with thiolutin (left panel) or thiolutin + cycloheximide (right panel), and samples were taken at the indicated time points. Relative m6A levels were determined by LC-MS. **(F)** m6A-ELISA comparing WT, *pho92*Δ and *not3*Δ signal before and after blocking transcription with thiolutin for 15 min. Cells were grown to be induced to enter meiosis (FW1511, FW3528 and FW6090). Cells were treated with thiolutin + cycloheximide, and samples were taken at 15 min after treatment. Relative m6A levels were determined by m6A-ELISA.

Figure 1

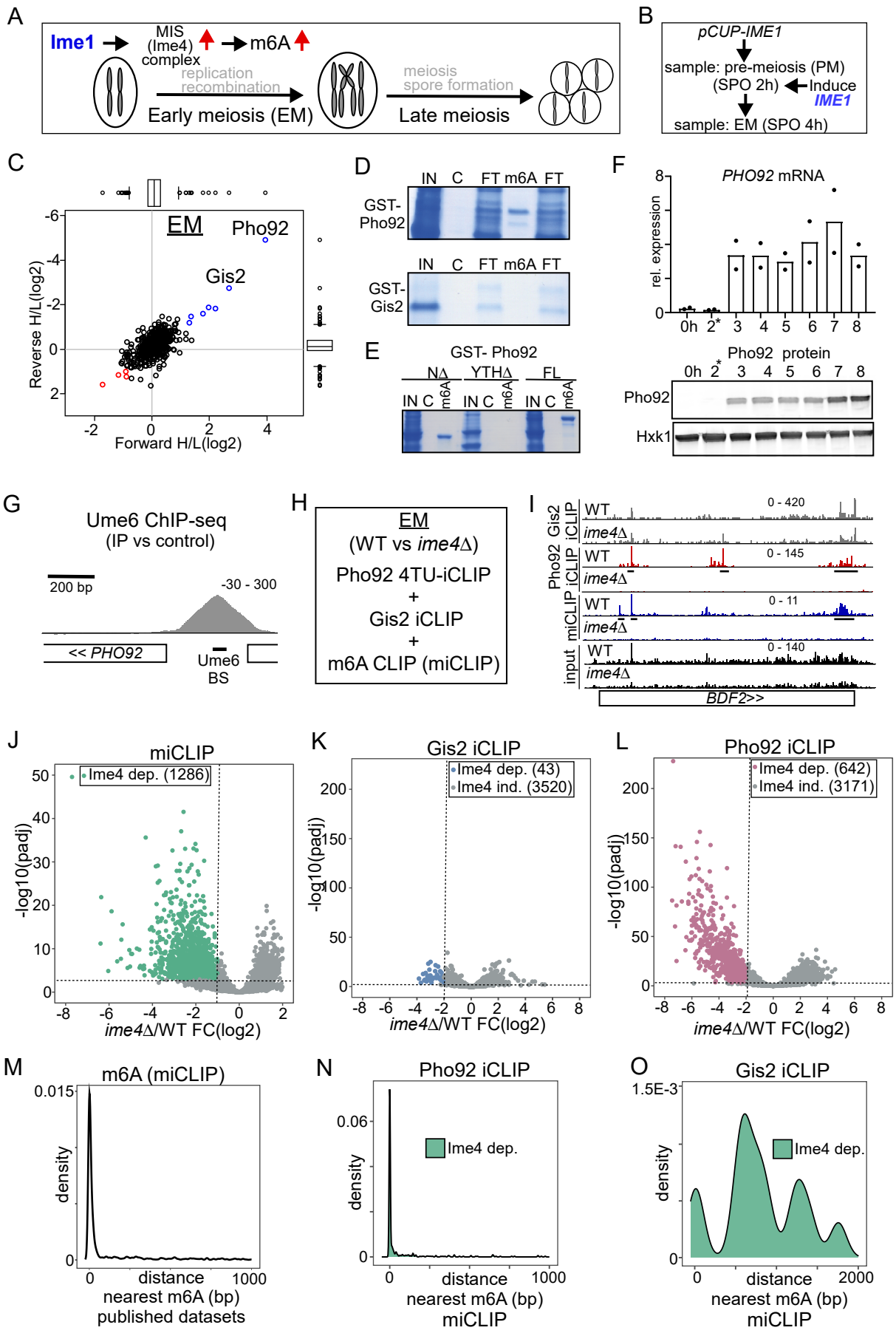

Figure S1

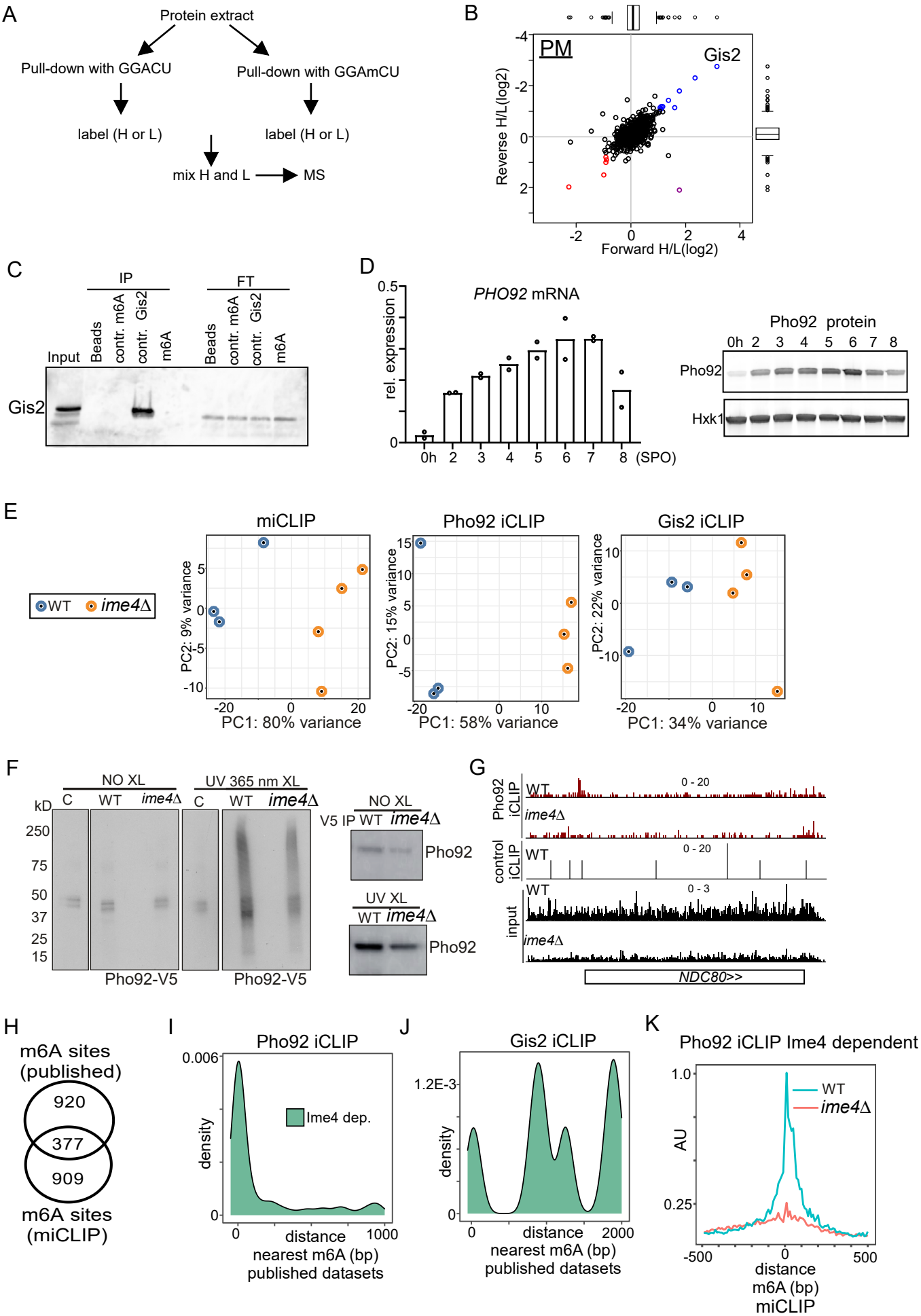

Figure 2

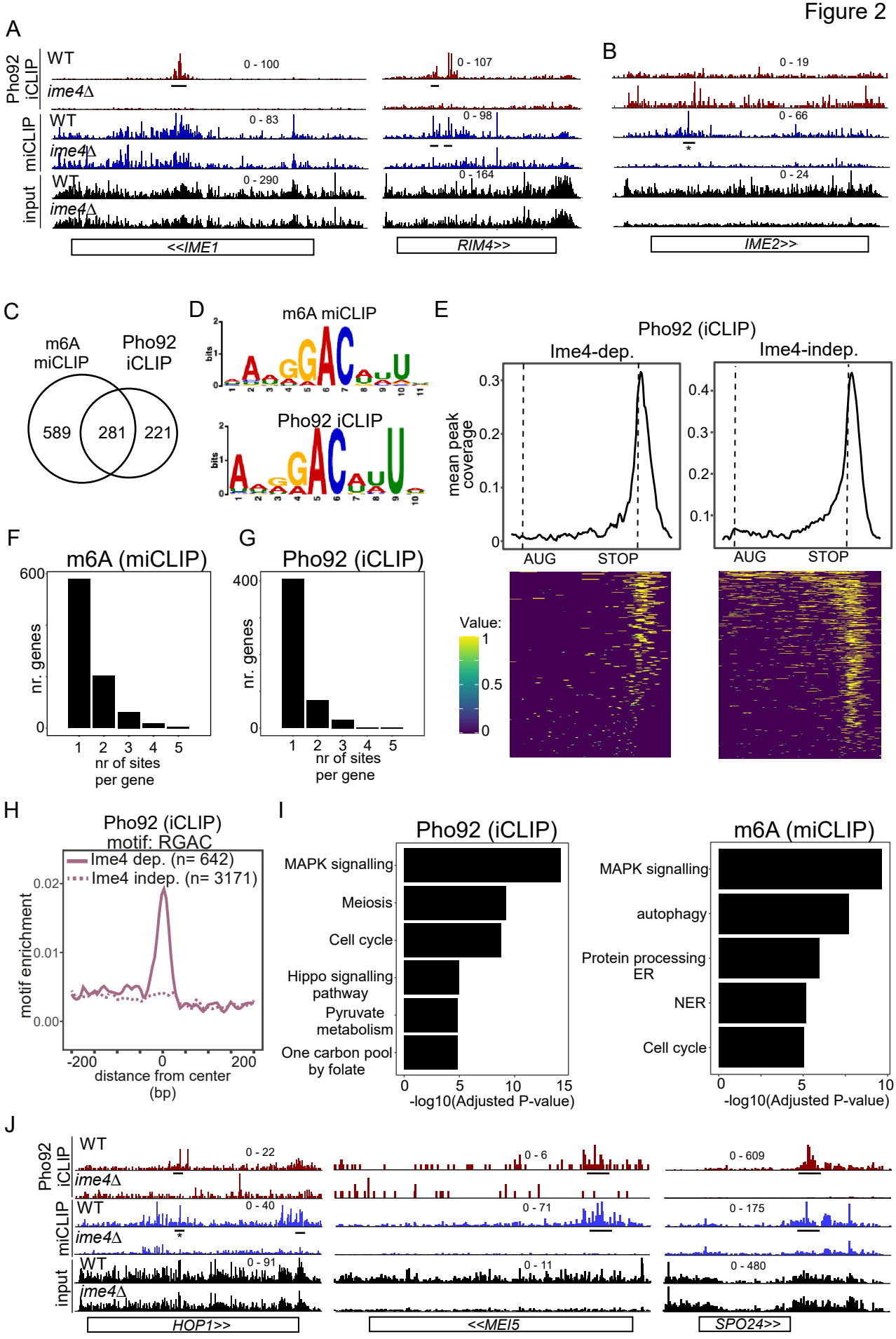

Figure S2

A

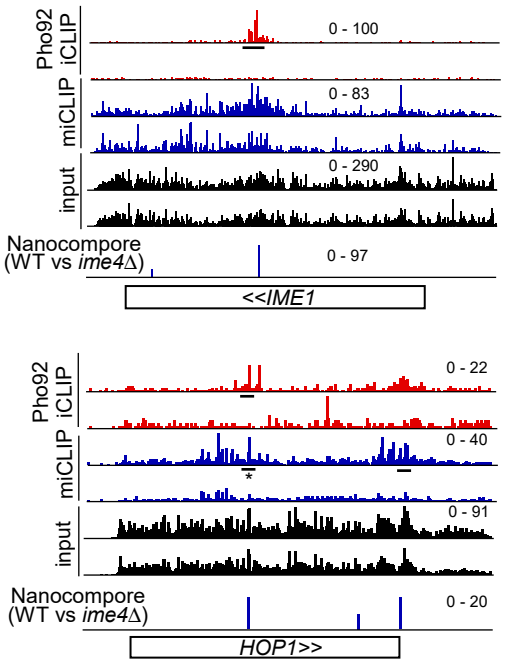

B

STREME: Pho92 CLIP Ime4 dependent

motif	P-value	E-value	nr sites (%)
AWRGACWUUW	2.2e-012	9.0e-012	412 (64.2%)
UAUAUAUAUGUAU	8.2e-002	3.3e-001	43 (6.7%)
UUCAUCCA	5.0e-001	2.0e+000	29 (4.5%)
AAAAAAAAAAUAAA	7.5e-001	3.0e+000	26 (4.0%)

STREME: m6A miCLIP

HAWGGACWWUW	9.5e-011	5.7e-010	874 (68.0%)
UGAUGAUG	3.5e-002	2.1e-001	200 (15.6%)
CCGAUG	4.2e-002	2.5e-001	69 (5.4%)
AACAAYGUUA	5.0e-001	3.0e+000	34 (2.6%)
AGAAUUUGAA	5.0e-001	3.0e+000	33 (2.6%)
GAAAAAAAAAA	8.8e-001	5.3e+000	37 (2.9%)

STREME: Pho92 CLIP Ime4 independent

GUGCCNY	2.6e-02	1.3e-01	436 (13.7%)
UUUUGUUU	3.9e-002	1.9e-001	1743 (55%)
UCUUGU	4.4e-001	2.2e+000	29 (8.9%)
UUCCG	4.6e-001	2.3e+000	26 (69%)

C

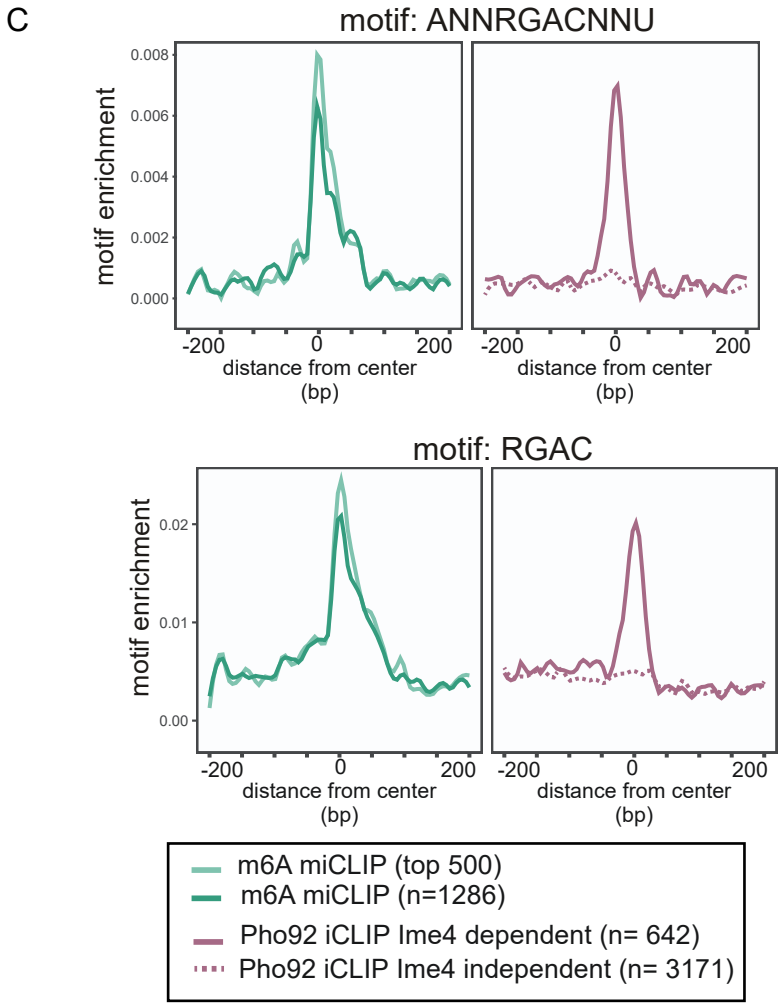

D

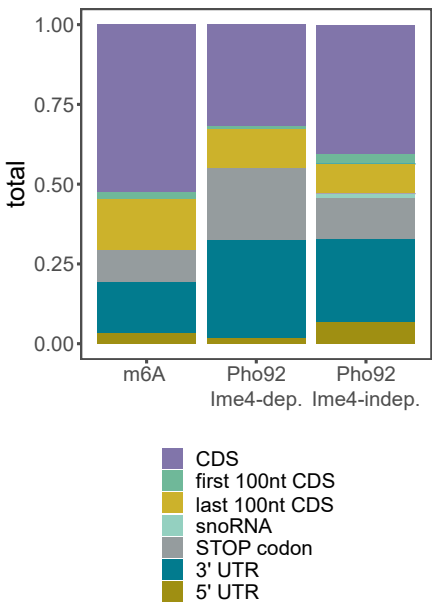

Figure 3

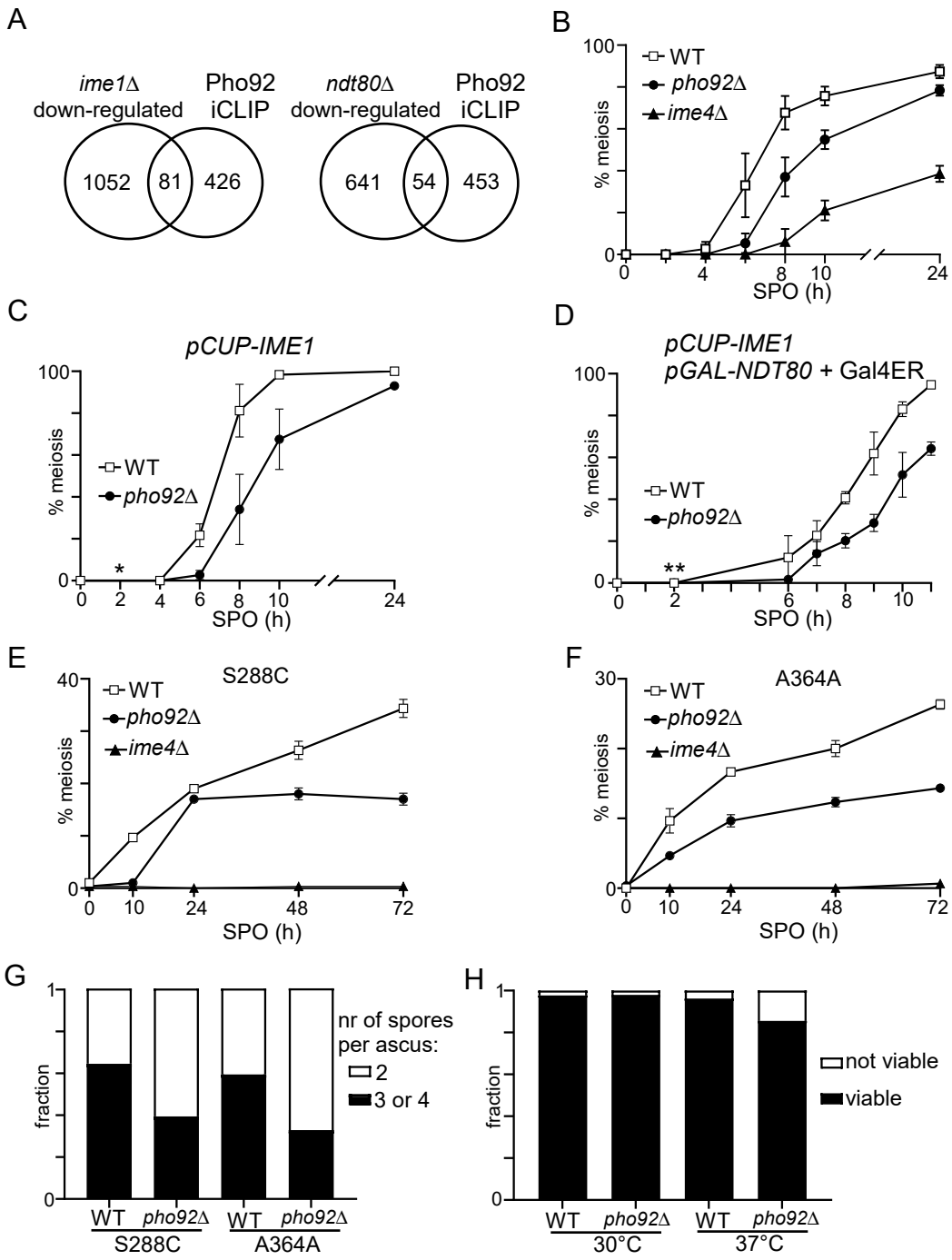

Figure S3

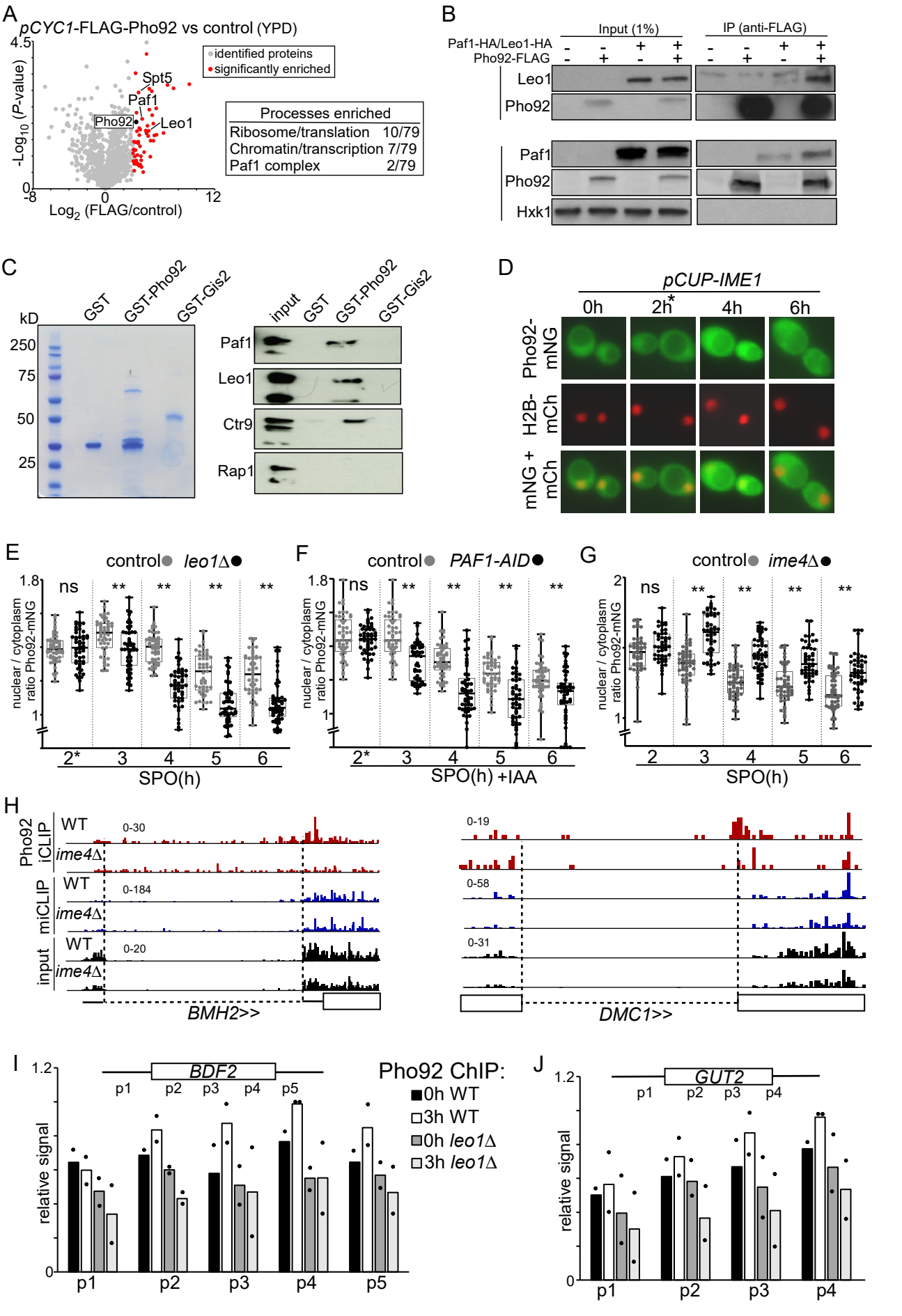

Figure S4

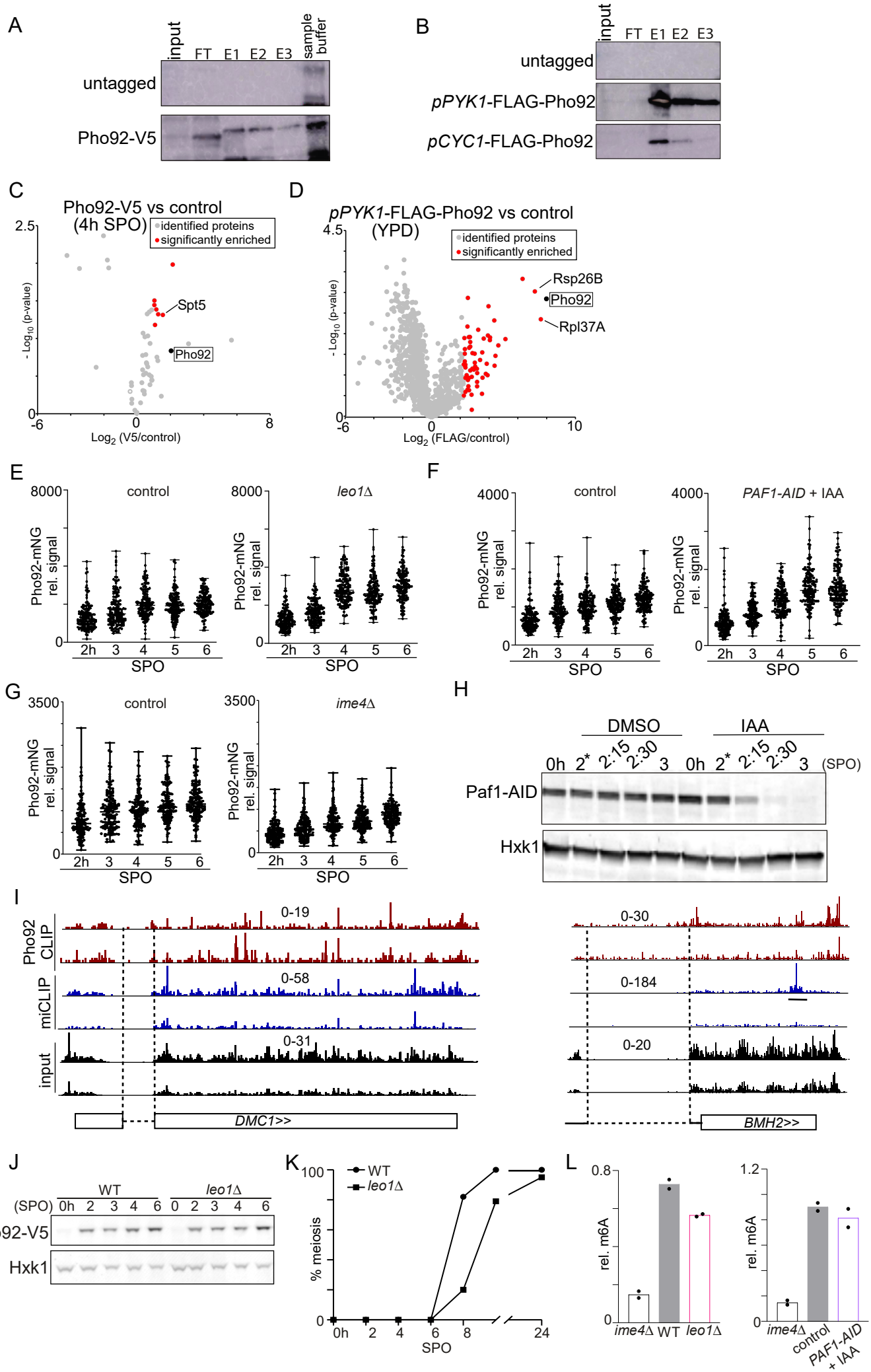

Figure 5

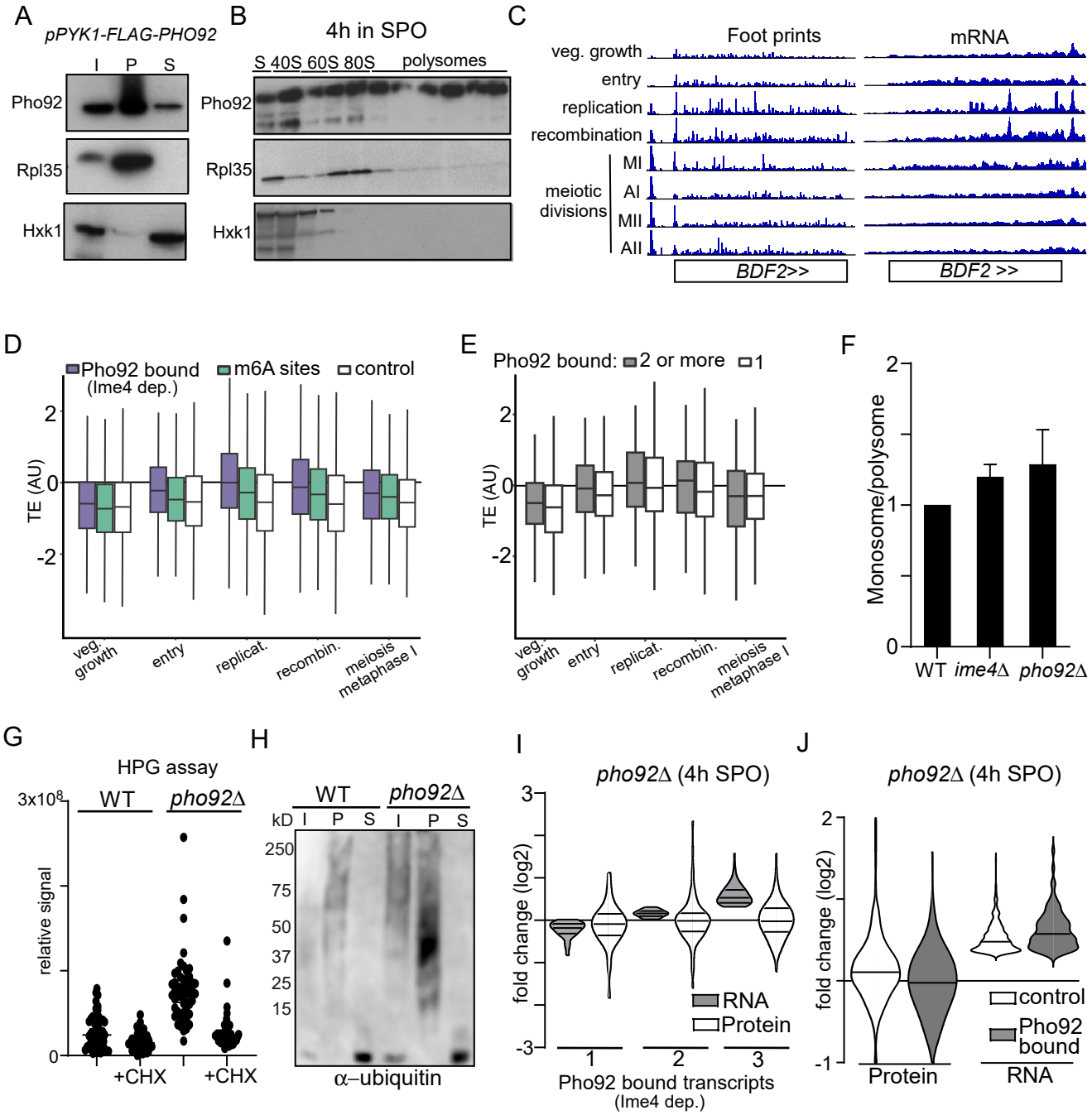

Figure S5

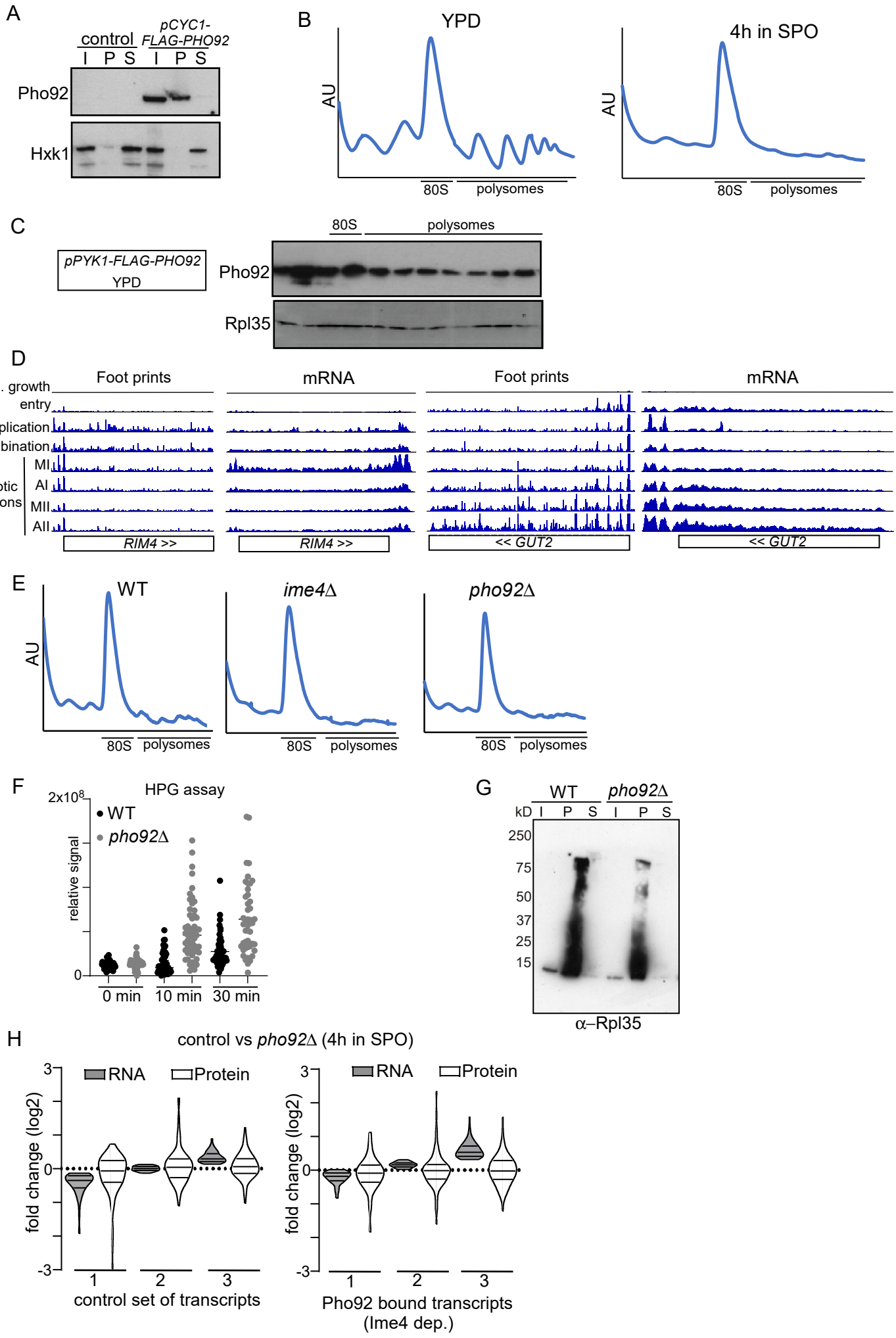

Figure 6

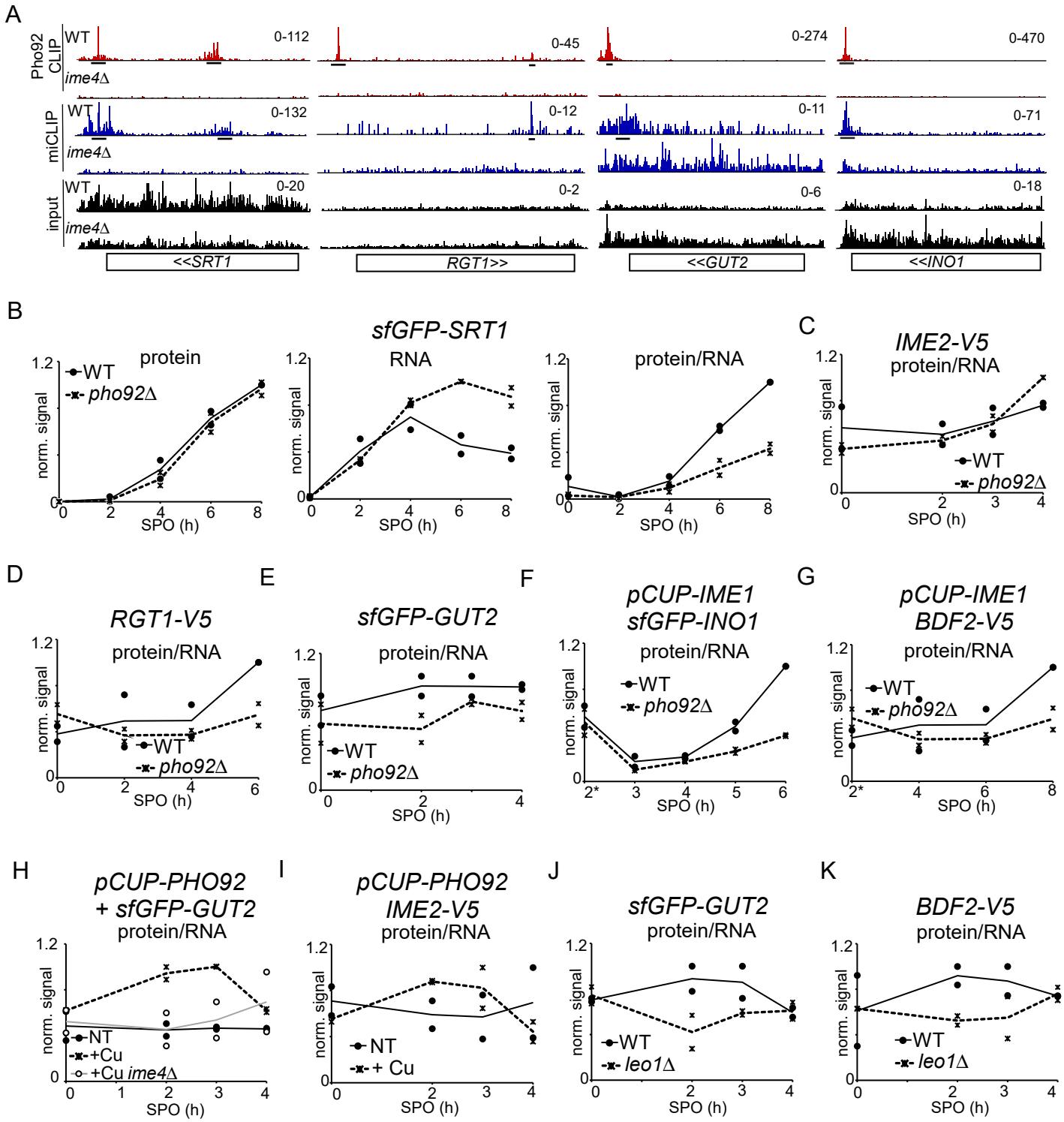

Figure S6

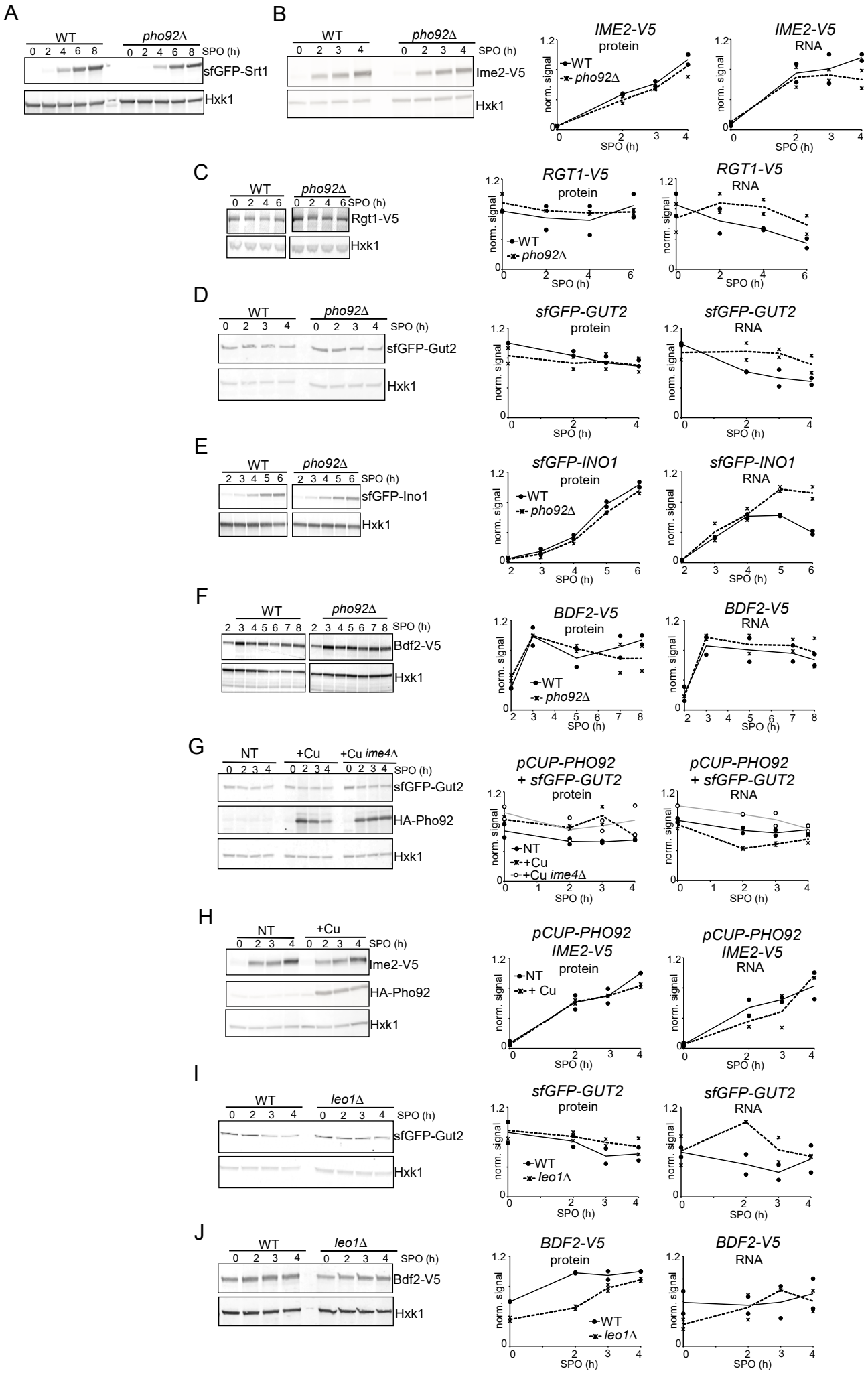

Figure 7

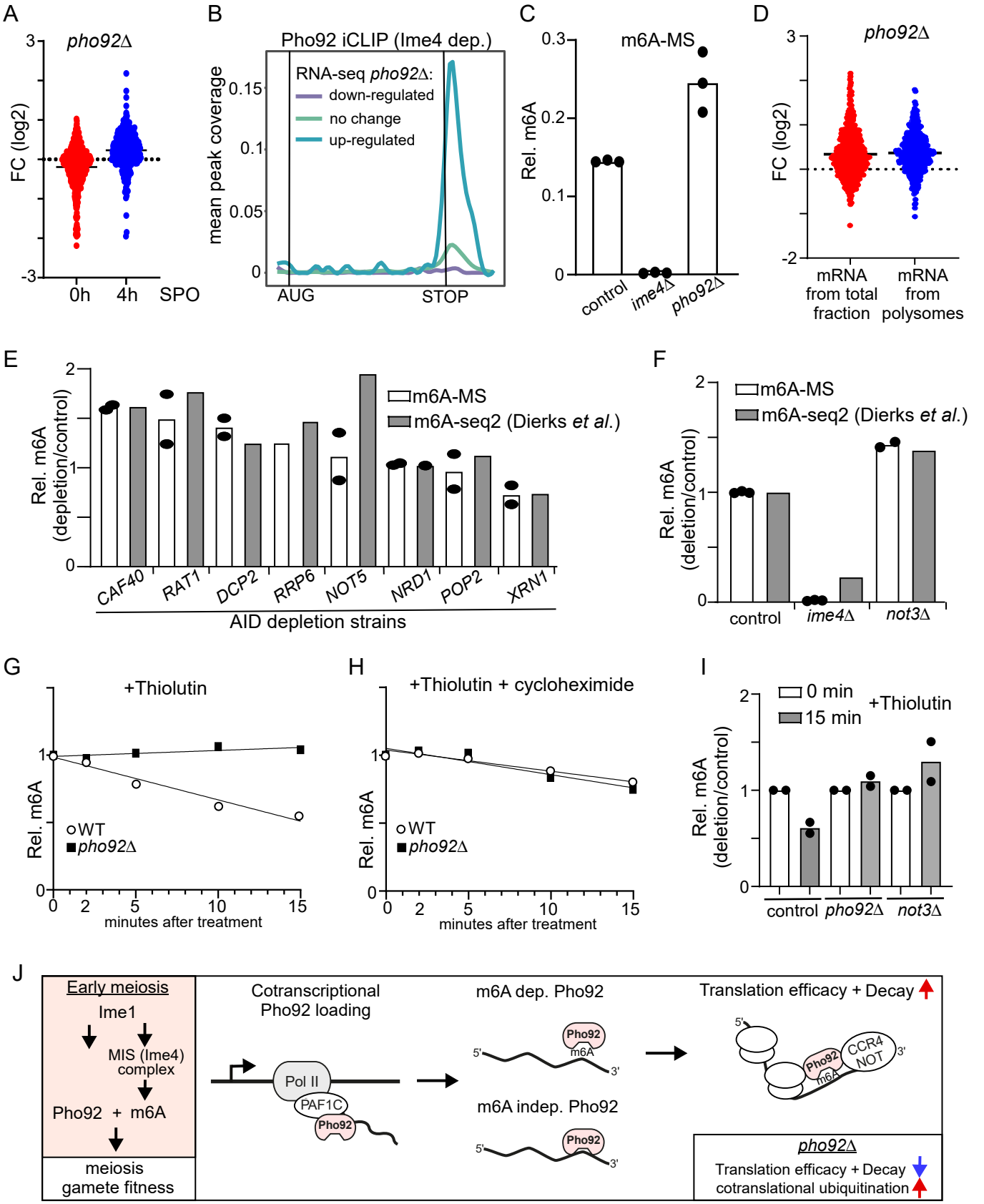

Figure S7